Part II
Enabling Technologies for Drivetrain and Gearbox Analysis

Chapter 8
OWT Drivetrain & Gearbox Simulation and Testing

Simone Manzato and Bert Pluymers

Abstract As wind turbines continue to grow in size and offshore installations become more and more attractive for investors, the design of reliable drivetrains and gearboxes is becoming very critical. One key element is represented by the challenging environmental conditions, which are significantly different and harsher than those experienced by onshore machines. Additionally, a deeper understanding of the operational loads and the effects of combined aero—and hydrodynamic forces on the drivetrain is essential to ensure the wind turbines can be guaranteed for the expected lifetime. These problems result in increased research efforts towards improving the capabilities and the use of simulation tools to better understand the complex drivetrain dynamic behavior. In parallel, advances in experimental techniques are also sought, as a way of deriving reliable information for model verification and validation, and to get a deeper insight in the structure operational response.

8.1 Simulation and Testing in Drivetrain and Gearbox Design

The drivetrain and the gearbox in particular continue to play a key role in the wind turbine industry. According to a report published online by OffshoreWIND.biz (2014), the global gearbox market increased from approximately $1.9 billion in 2006 to $4.0 in 2013, thanks in particular to the significant increase in installed power worldwide. However, direct-drive solutions are attracting more and more the interest of the manufacturers and it is expected that the market share of the two solutions (displayed in Fig. 8.1) will soon be balanced.

S. Manzato (✉)
Siemens Industry Software (SISW), Interleuvenlaan 68, 3001 Leuven, Belgium
e-mail: simone.manzato@siemens.com

B. Pluymers
Department of Mechanical Engineering, KU Leuven, Celestijnenlaan 300c, 3001 Leuven, Belgium
e-mail: bert.pluymers@kuleuven.be

W. Ostachowicz et al. (eds.), *MARE-WINT*, DOI 10.1007/978-3-319-39095-6_8

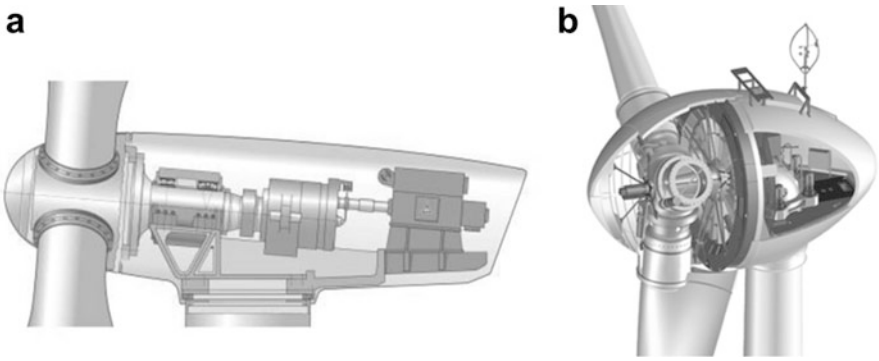

Fig. 8.1 Typical turbine driveline configurations. (**a**) Gearbox and (**b**) Direct-drive generator

Gearboxes typically have the advantage of requiring smaller initial investments, but because of the number of rotating parts, gear pairs and bearings, reliability is typically an issue. On the other hand, direct-drive machines require a bigger investment related to the development and construction of big permanent magnet generators but have typically lower operation and maintenance costs. To guarantee the effectiveness and competitiveness of the gearbox solution, significant improvements in the design phase are required to better understand the mechanisms leading to gearbox failures. This can only be achieved by developing more accurate, reliable and efficient numerical models, able to replicate not only the global load transfer paths across the driveline but also the local load transfer mechanisms.

More advanced design tools are not only motivated by the call for reliability, but also by other technological drivers which makes the role of the drivetrain more and more critical. As extensively discussed by Helsen et al. (2012), turbine manufacturers are aiming at developing ever bigger machines, with the objective of maximizing the power produced by each individual machine. This trend, over the past 30 years, is shown in Fig. 8.2: bigger and longer blades installed on higher turbines will give access to higher wind speeds and consequently increase the generated power. However, this also poses critical design challenges. Bigger wind turbines and corresponding bigger blades impose higher loads on the turbine components, and in particular the drivetrains, and these loads cannot be considered quasi-static as in the majority of industrial applications. These loads represent a combination of aerodynamic loads at variable wind speeds, gravitational loads and corresponding bending moments, inertial loads due to acceleration, centrifugal and gyroscopic effects, generator torque loads and loads introduced by control actions such as blade pitching, starting up, emergency braking and yawing. Besides, driveline is also subjected to transient phenomena related to sudden wind gusts or electrical grid malfunctioning which generates heavy loads on all rotating components, and in particular on gears and bearing. These effects contribute to non-torque loading, where vertical, horizontal and axial loads are applied on the gears and bearings. Neglecting these effects in design phase is one of the causes of premature failure of gearboxes components, in particular bearings and gears.

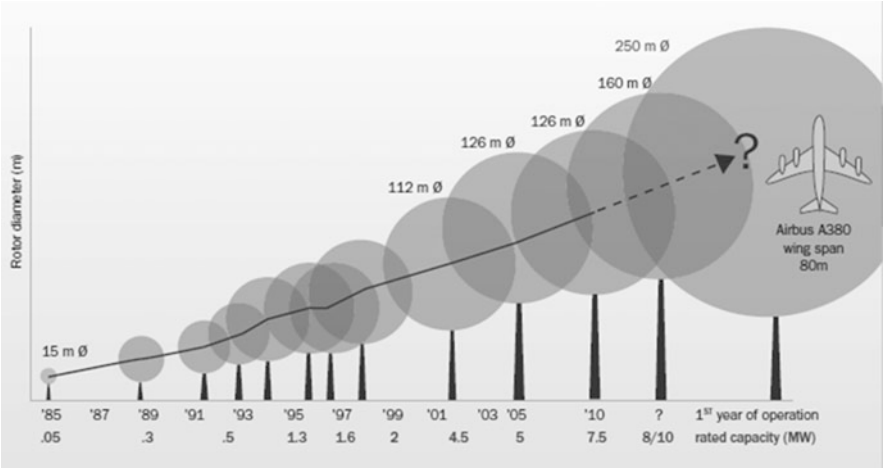

Fig. 8.2 Wind turbine upscaling trend over the past 30 years (*Source*: FP6 Upwind project, 2011)

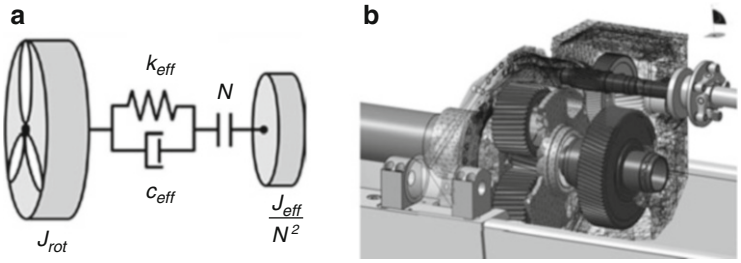

Fig. 8.3 Modelling approaches for wind turbine gearboxes. (**a**) two DOFs torsional model from Girsang et al. (2013), (**b**) flexible MBS model of the NREL GRC gearbox

Over the past decade, gearbox manufacturers have recognized the limitations related to common design approaches and started integrating more and more numerical tools to validate innovative designs. This paradigm shift represents the foundation of the work by Peeters (2006), where the limitations in traditional design codes for wind turbine design were identified. The work reviews state-of-the-art design tools for wind turbine drivetrain in the early 2000 and introduces a new modelling approach for the simulation of more detailed drivetrain loads relying on the flexible Multibody Simulation (MBS) approach. Two of the discussed modelling approaches, going from two to thousands of degrees of freedom, are shown in Fig. 8.3. The work focused on the importance of modelling the internal dynamics in the gearbox and the complex interaction between the different subcomponents to be able to correctly estimate the operational loads and consequently include this information in the design phase.

The conclusion of Peeters (2006) paved the way for further developments and optimization in the modelling strategies of gearboxes. In the work of Helsen (2012)

efficient simulation strategies have been investigated to understand the interaction of the turbine transients with the dynamic excitation within the drivetrain originating from the meshing gears and the full drivetrain structural behavior. The importance of modelling dynamic flexibility of internal gearbox components such as the ring wheel and the planet carrier(s) has also been investigated. Advanced model order reduction techniques based on static mode switching (Tamarozzi et al. 2013) have been applied to accurately simulate a 3D gear contact problem. The results show that the method is able to keep the same level of accuracy of fully non-linear simulation models while drastically reducing the computational resources. Finally, the recent work of Vanhollebeke (2015) demonstrated the possibility to use very accurate flexible MBS models of gearbox and to integrate them in the design phase not only to accurately predict loads but also to efficiently analyze possible NVH problems such as tonalities and vibrations.

Within the MAREWINT project, specific activities were conducted to follow up on these findings and complement the existing work with focus on two specific aspects. Chapter 9 focuses on a review of advanced modelling techniques for bearing and the optimal integration of these models in a flexible multibody simulation environment. In Chap. 10, recent advances on the experimental characterization of gearboxes in operations are presented. Being able to identify an operational model of the gearbox under different loading conditions will provide valuable inputs for validation of global gearbox models and verification of design assumptions.

References

Girsang IP, Dhupia JS, Muljadi E et al (2013) Gearbox and drivetrain models to study dynamic effects of modern wind turbines. Paper presented at the IEEE energy conversion congress and exposition Denver, 15–19 September 2013

Helsen J (2012) The dynamics of high power density gear units with focus on the wind turbine application. Dissertation, KU Leuven

Helsen J, Vanhollebeke F, Vandepitte D et al (2012) Some trends and challenges in wind turbine upscaling. In: Abstracts of the ISMA 2012, international conference on noise and vibration engineering, Leuven, 17–19 September 2012

OffshoreWIND.biz (2014) Report on Wind Turbine Gearbox and Direct-Drive Systems out now. http://www.offshorewind.biz/2014/09/19/report-on-wind-turbine-gearbox-and-direct-drive-systems-out-now/. Accessed 19 Jan 2016

Peeters J (2006) Simulation of dynamic drive train loads in a wind turbine. Dissertation, KU Leuven

Tamarozzi T, Ziegler P, Eberhard P et al (2013) Static modes switching in gear contact simulation. Mech Mach Theory 62:69–106. doi:10.1016/j.mechmachtheory.2013.01.006

Vanhollebeke F (2015) Dynamic analysis of a wind turbine gearbox: towards prediction of mechanical tonalities. Dissertation, KU Leuven

Chapter 9
Dynamic Behavior of Bearings on Offshore Wind Turbine Gearboxes

Rubén Cerdá, Bart Blockmans, Jakob Fiszer, Tommaso Tamarozzi, Bert Pluymers, and Wim Desmet

Abstract Gearbox failure is among the highest causes of downtime in a wind turbine, causing a significant loss to the wind energy sector, especially in the complex offshore environment. Quite often, the cause of these gearbox and drivetrain errors, as well as other undesired noise and vibrations issues, is premature bearing failure. Therefore, developing more efficient and reliable bearing models and simulation methods that can accurately predict the nonlinear dynamic loads already in the design phase is still crucial. Without claims of completeness, a few important items to be considered when analyzing bearings and a state-of-the art review for bearing modelling approaches (from analytical lumped parameter models to complex flexible multibody simulations) will be discussed in this chapter. Furthermore, some recent modelling developments and the problem of integrating these bearing models with similar advanced gear models into flexible multibody simulations at full-scale wind turbine drivetrain level will be addressed.

9.1 Introduction

Improving the reliability of wind turbines (WT) is an essential component in the bid to minimize the cost of energy (COE) from wind, especially for offshore wind turbines because of the difficulties associated with access for maintenance. Unfortunately, many drivetrains are suffering premature bearing failures. These bearing failures are very costly, particularly given the long downtime incurred per failure. Numerous studies have been undertaken to obtain the distribution of failures by assembly in WTs. Gearbox and generator failure rates remain unacceptably high. Furthermore, the downtime for these failures is amongst the highest of all WT assemblies. Often the entire gearbox or generator needs to be replaced, which requires the deployment of a large crane. These cranes are costly and may take days or weeks to deploy. Offshore, it is not unusual for rough weather to prevent access

R. Cerdá (✉) • B. Blockmans • J. Fiszer • T. Tamarozzi • B. Pluymers • W. Desmet
Department of Mechanical Engineering, KU Leuven, Celestijnenlaan 300c, 3001 Leuven, Belgium
e-mail: ruben.cerda@kuleuven.be; bart.blockmans@kuleuven.be; jakob.fiszer@kuleuven.be; tommaso.tamarozzi@kuleuven.be; bert.pluymers@kuleuven.be; wim.desmet@kuleuven.be

W. Ostachowicz et al. (eds.), *MARE-WINT*, DOI 10.1007/978-3-319-39095-6_9

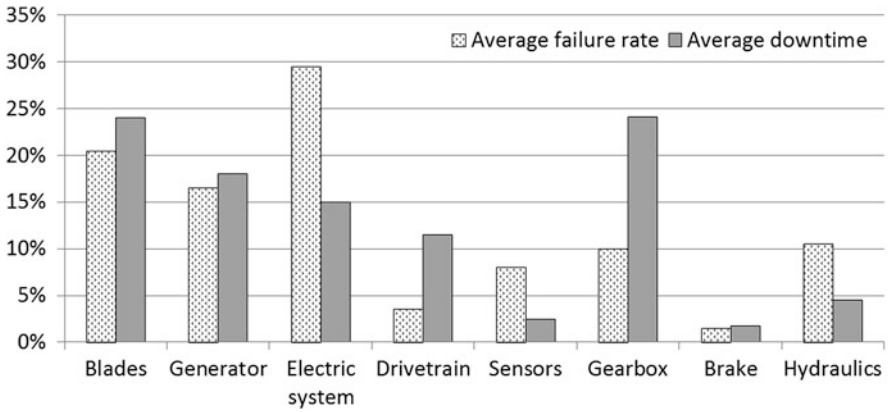

Fig. 9.1 Distribution of failures and downtime by assembly in WT (adapted from EWEA 2011)

for operation and maintenance for weeks at a time. Figure 9.1 shows the average failure rate and the incurred average downtime by assembly, based on the work presented in EWEA (2011).

Moreover, Chen and Alewine (2010) published the findings of a survey of over 800 failed WT generators, which showed that the dominant source in multi-megawatt WT generators is the bearing. Despite this evidence, and although the unique operational conditions of the bearings resulting from widely varying wind loads and high vibration levels are well known, the root causes of these failure data are not completely known. There is, therefore, a need to search for more accurate and trustworthy component-level models and to undertake full dynamic multibody simulations at WT drivetrain system level.

Mechanical transmissions have been continuously attracting the interest of researchers and engineers, who dedicated consistent resources and efforts since the second half of the past century to investigate the multiple and interconnected phenomena that are typical in transmission dynamics. However, despite extensive studies in the last decades, system-level dynamics for the whole mechanical transmission is gaining a game-changer role and requires a deeper understanding and a more detailed knowledge to allow designers to address at the same time efficiency, durability and noise predictions and optimization.

Current simulation techniques rely on the assumption that the components are rigid, or adopt linearized modal reductions, which are applicable for the shafts and the housing but introduce significant approximations for the other components since they do not allow modelling the nonlinear dynamic contact interactions involved in the gear meshing and in the bearings with sufficient accuracy if a lumped-parameters approach is used.

Due to the highlighted reasons, the design of a WT drivetrain that is optimized from the dynamic point of view at a system level can be achieved only by establishing a simulation methodology that is capable of capturing, in a multi-discipline

integrated, detailed yet computationally efficient way, all those phenomena that are relevant for the non-linear dynamic behavior of the system.

9.2 Bearings for Wind Turbine Applications

Besides gears, bearings are the other main sub-system in every mechanical transmission. Due to the great variety of bearing types, the scope of this section is narrowed down to rolling-element bearings (also known as rolling or roller bearings). This type of bearing is one of the most used in mechanical applications, playing a crucial and effective role across various industries such as automotive or wind turbines.

In this section, some of the main phenomena affecting bearings, with a specific focus on wind turbine applications, are discussed.

9.2.1 Rolling-Element Bearings: Basic Concepts

The term "rolling" is collectively used for all forms of bearings that utilize the rolling action of balls or rollers to minimize the friction from a constrained motion of one body relative to another. Most bearings provide a close relative position of two loaded components yet allow a rotational motion between them. Special types only allow a linear motion in the direction of a stationary shaft (e.g. linear guides). A combination of both degrees of freedom is also possible. Various types of rolling elements are available to achieve this constrained motion. They can be categorized into five standard shapes: ball bearing, cylindrical bearing, tapered bearing, needle bearing and barrel bearing; each suitable for a different application.

A common rolling element bearing typically consists of an inner and an outer ring and a number of rolling elements which form the connection between the rings. The rolling elements are often guided by a cage to ensure uniform distribution and to prevent mutual contact. To prevent axial motion of the elements, both the inner and outer ring of most ball bearings include a gap called groove or raceway. Besides constraining the axial motion, the raceways also store the lubrication, which is necessary in order to reduce the friction and wear in the rolling contacts. A seal is also implemented to contain the lubricant and protect the raceway from dirt.

A more extensive version of this brief introduction to the nomenclature of rolling bearings can be found in Harris and Kotzalas (2006) and Wensing (1998).

The need to reduce vibrations of rotating machinery has stimulated researchers for many years to analyze the dynamic behavior of rolling element bearings. As the bearings are in the transmission path of vibrations between the shaft and bearing housing, they play a key role in the resulting vibrations. They determine for instance the machine's critical speeds and the forces acting on the different components. Subsequently, they influence the noise emanating from the machine and component

stresses and wear. Some of the main phenomena that affect the non-linear dynamic behavior of the bearings are discussed in the following subsections.

9.2.2 Contact Mechanics

When two elastic solids contact under a load *w*, a contact area develops. In many engineering applications such as rolling element bearings and gears, the contact area is small and the resulting pressure is high. The local deformation and stresses can be determined from analytical formulas, based on the theory of elasticity and derived by Hertz. Hertz's contact model is based on the following assumptions (Wensing 1998):

- The material deformation is elastic.
- The load is directed normally to the contacting surfaces, such that surface shear stresses can be neglected.
- The dimensions of the contact area are small compared to the radii of curvature of the contacting bodies.
- The effect of surface roughness is negligible.

For a point contact in ball bearings, an elliptical shape of the contact area is assumed. Figure 9.2 shows the contact geometry (Jacobs 2014). The rolling element load *w* is oriented in the x-direction, the rolling direction equals the y-direction and the bearing's rotation axis is oriented in the z-direction. The contact is characterized by its radii of curvature in two principal planes, perpendicular to each other. The first principal plane (xz-plane) contains the bearing's rotation axis and a rolling element center. The semi-major axis of the elliptical contact *a* is located in this plane. The

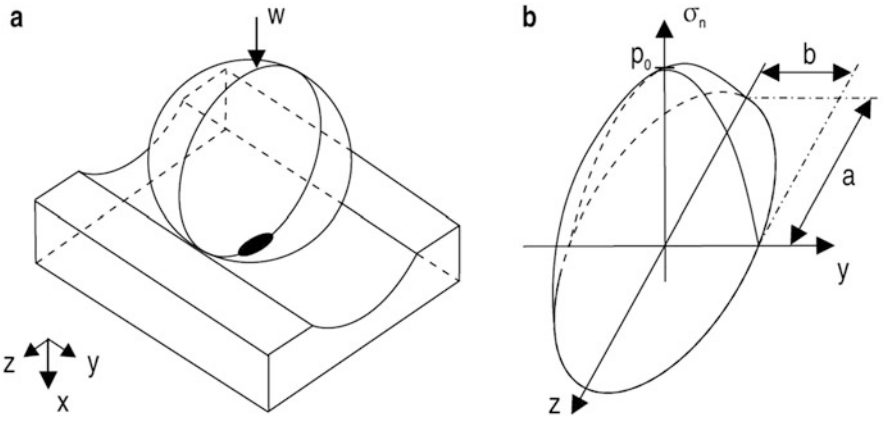

Fig. 9.2 (**a**) Elliptical contact area in *black* and in (**b**) the corresponding surface stress distribution (Jacobs 2014)

second principal plane (xy-plane) is perpendicular to the rotation axis and contains a rolling element center. The semi-minor axis of the elliptical contact b is located in this plane.

The contact problem is reduced to the problem of a paraboloid shaped surface approaching a flat surface. The normal stress is distributed over the contact area in the form of a semi ellipsoid, as shown in Fig. 9.2b. The maximum normal stress at the surface p_0 occurs at the geometrical center of the contact area and thus amounts to 1.5 times the evenly distributed pressure:

$$p_0 = 1.5\frac{w}{A} \tag{9.1}$$

where the contact surface area A is given by:

$$A = \pi \cdot a \cdot b \tag{9.2}$$

with a and b being the semi-major and semi-minor axis of the elliptical contact.

This maximum stress is also called maximum Hertzian contact pressure. The normal stress σ_n at all other points within the contact area is given by:

$$\sigma_n = p_0\left(1 - \left(\frac{z}{a}\right)^2 - \left(\frac{y}{b}\right)^2\right)^{1/2} \tag{9.3}$$

Beside the surface stresses caused by a concentrated force applied perpendicular to the surface, rolling contacts of ball bearings also have subsurface stresses. The principal stresses occurring below the center of the contact area were calculated by Jones (1946). Based on Mohr's circle, the maximum shear stress is derived as well. Due to friction between the rolling elements and raceways, tangential forces are introduced on the surface. The effect of the resulting surface shear stress on the subsurface stresses was analyzed by Zwirlein and Schlicht (1980).

9.2.3 Influence of the Lubricant Film

The first realistic model which provided an approximate solution for the lubricant film thickness was proposed by Grubin (1949). It was found that the combination of three effects is instrumental to the lubrication mechanism: hydrodynamic lubrication, elastic deformation of the metal surfaces and the increase in viscosity of oil under extreme pressures. It was shown theoretically that under the condition of intense contact stress, a lubricating oil film can be formed. This elasto-hydrodynamic lubrication (EHL) film is very thin (0.1–1 μm), but separates the interacting surfaces.

In a stationary contact between a ball and raceway, the pressure distribution is ellipsoidal according to the classical Hertzian theory (Fig. 9.2b). The pressure field

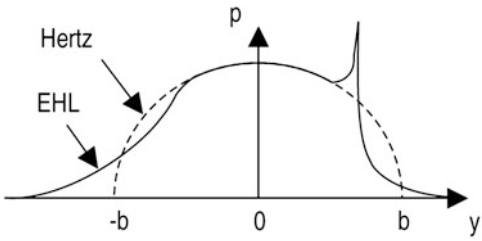

Fig. 9.3 Pressure distribution considering the EHL film (Jacobs 2014)

changes when the lubricant is dragged into the contact with a mean velocity. An EHL film is generated, which modifies the pressure distribution at the entry and exit regions of the contact. Figure 9.3 (Jacobs 2014) shows the pressure distribution along the minor axis of the elliptical contact.

Due to the strong interaction between the EHL film and the deformation of the contacting surfaces, the lubricant film affects the stiffness and damping characteristics of the bearing.

One of the most up-to-date analyses of the stiffness and damping evaluation for elasto-hydrodynamic contacts is based on the assessment of the dynamic response through a full dynamic simulation of the contact forces. It was first published by Wijnant (1998) and later extended by Wensing (1998) and Nonato and Cavalca (2012). Owing to the formation of a lubricant film, an increasing stiffness of each contact in comparison to a dry contact is observed. Also, the effective internal bearing clearance is reduced. The formation of a lubricant film consequently leads to an increased bearing stiffness.

Experimental studies analyze the variations of the bearing dynamics for different values of the load, speed and lubricant's viscosity. Dietl et al. (2000) measure the damping capabilities of two rolling element bearings supporting a rigid shaft. Mitsuya et al. (1998) investigate the damping characteristics of a single deep groove ball bearing. A higher damping of the lubricated bearing in comparison to a dry bearing is observed in each publication. The difficulty of performing sufficiently accurate measurements and the multitude of parameters influencing the results (type of bearings, radial and axial preload, speed, loose/interference fits of the bearing seats, lubricant properties, temperature, etc.) is emphasized in most of these publications.

9.2.4 Durability

Rolling elements bearing failure is one of the foremost causes of breakdown in rotating machinery (Li et al. 1999). Bearings fail prematurely in service due to phenomena like contamination, poor lubrication, poor fits, misalignments, etc. The main contributors to the decrease in the durability of a rolling bearing are the behavior of the lubricant film during strong external excitation and the damage of

the raceway surfaces due to the external dynamic loads that can be applied to the bearing for a long period of time.

Common Fatigue Failure Modes Every rolling element bearing rotating under load above the endurance strength limit has a definite fatigue life. The bearing approaches the end of its life when the rolling surfaces are damaged by rolling contact fatigue (RCF). Two mechanisms of fatigue damage initiation can be distinguished (Muro and Tsushima 1970):

- *The subsurface failure mode*: In many applications, the lubrication of the rolling contacts is adequate and the friction between the rolling elements and raceways is negligible. The von Mises equivalent stress reaches its maximum at a point below the surface. The stress can locally exceed the yield strength of the bearing steel (between 1400 and 1800 MPa) such that plastic deformation occurs. During cyclic loading, residual stresses build up and minute cracks are formed below the surface. This is often observed in the region of material inhomogeneities, where the stresses are maximal. The subsurface cracks eventually progress towards the surface. Surface material can break loose such that deep spalls are formed. During the remaining bearing lifetime, the damage spreads rapidly since torn-off particles are rolled over causing local overloading. A detrimentally preloaded bearing, for instance due to poor fits or misalignment, fails prematurely due to RCF initiated below the surface.
- *The surface failure mode*: Ceramic or metallic foreign solid particles contaminate the lubricant in the contacts. The solid particles originate for instance from the grinding process of the bearing and/or its surrounding structure (carbide cluster). Due to over-rolling during the bearing operation, indentations on the raceway surfaces are formed. The Hertzian micro-contacts between the surfaces and the solid particles are subjected to cyclic loading. This results in increasing residual stresses near the surface up to a depth related to the size distribution of the indentations. Strain hardening by severe plastic deformation leads to material embrittlement and subsequent crack initiation on the surface. Further failure development produces shallow V-shaped pits which are originally only several micrometers deep. The pits are formed behind the indentations. Chips of surface material flake off causing accelerated wear. While a small amount of wear is natural and unavoidable in most bearing arrangements, inadequate sealing and defective lubrication lead to severe wear. The bearing fails prematurely due to RCF initiated at the surface.

Lifetime Calculation Accurate prediction of the lifetime of rolling element bearings is a crucial step towards a reliable design of many rotating machines. The general lifetime calculations are based on the assumption that the rolling surfaces flake sooner or later due to RCF initiated below the surface (subsurface failure mode). According to the classical fatigue theory, the first cracks usually emanate from inhomogeneities in the material, such as microscopically small inclusions or metallurgical dislocations. In recent years, inhomogeneities in the bearing material became less important as a cause of fatigue damage, owing to the

constant improvement of the material cleanliness. Today, most cracks emanate from indentations caused by solid particles (surface failure mode). The inhomogeneities are randomly distributed in the material and vary in size and type. The solid particles may enter rolling contact areas at an earlier or later time. With identical bearings and operating conditions, fatigue damage therefore occurs after different periods of operation. Brandlein et al. (1999) describe a series of lifetime tests. Thirty bearings of the same batch are loaded in the same way till failure. Differences in lifetime up to a factor 20 are observed.

The wide scatter of running times explains the impossibility to accurately predict the lifetime of an individual bearing. Predictions can only be made for a large group of nominally identical bearings stressed in the same manner. The rating life L_{10} is defined as the running time at which 10 % of the bearings have failed. The ISO 281 standard gives the general equation for lifetime calculations, used for bearing dimensioning (ISO 2007):

$$L_{10} = \left(\frac{C}{P}\right)^p \tag{9.4}$$

where P is the equivalent dynamic load which takes into account both the radial and axial bearing load. The dynamic load rating C corresponds to a pure radial constant load at which the L_{10} life equals one million revolutions. The exponent p equals 3 for ball bearings. The rating life L_{10} is expressed in million revolutions.

When a bearing is not stressed beyond its endurance strength limit and the operating conditions meet certain prerequisites with regard to the lubricant film thickness and cleanliness of the lubricating gap, it does not fail. Also, the bearing life not only depends on the load. Other influences, such as the lubrication condition, have a significant effect. These aspects are not taken into account by Eq. (9.4). However, the equation remains the basis of bearing dimensioning and the starting point for adjusted calculation methods. Since the 1970s, empirical factors are added to the equation, considering the endurance strength limit, the lubrication condition, etc. In many bearing arrangements, the load and rotational speed change either randomly or according to a work cycle. An equivalent dynamic load is then calculated based on a series of individual loads and speeds of a certain duration q_i. This calculation is derived from the Palmgren-Miner rule of variable amplitude loading in the classical fatigue theory. With the rotational speed n_i when the load P_i is acting on the bearing and the mean rotational speed n_m, the equivalent dynamic load equals:

$$P = \left(\frac{\sum_{i=1}^{k} n_i q_i P_i^p}{n_m}\right)^{1/p} \tag{9.5}$$

Effect of External Dynamic Loads For bearings subjected to highly varying loads, recent research emphasizes a strong reduction of the actual bearing lifetime w.r.t. the calculated bearing lifetime. The influence of external dynamic loads on the lifetime of bearings is elaborately analyzed by Gegner (2011), and Nierlich and Gegner (2011). Cylindrical roller bearings are tested under high dynamic load using a novel bearing test rig. Due to axial vibrations, asperities of the contacting bodies experience strong sliding motion. Material aging is shifted towards the surface. This type of damage is not covered by the classical bearing lifetime calculations. Reductions of the actual L_{10} bearing life of 80 % w.r.t. the calculated lifetime are estimated.

9.2.5 Non Torque Loading

Non-torque loads include pitching moments caused by the rotor weight and tower shadow, wind-induced moments, moments caused by the controller, thrust, etc. Guo et al. (2014) and Park et al. (2013) have investigated the effects of non-torque loads, gravity and bearing clearance in the load-sharing and planetary loads of a three-point suspension wind turbine drivetrain. Non-torque loads affect gear and bearing loads and planetary gear load sharing. It is present on all the different drivetrain configurations: 3-point suspension (Fig. 9.4), 2-point suspension and on integrated gearboxes.

An analytical formulation was developed and a 3D dynamic drivetrain model that included mesh stiffness variation, tooth modifications and gearbox housing flexibility was built (Guo et al. 2014).

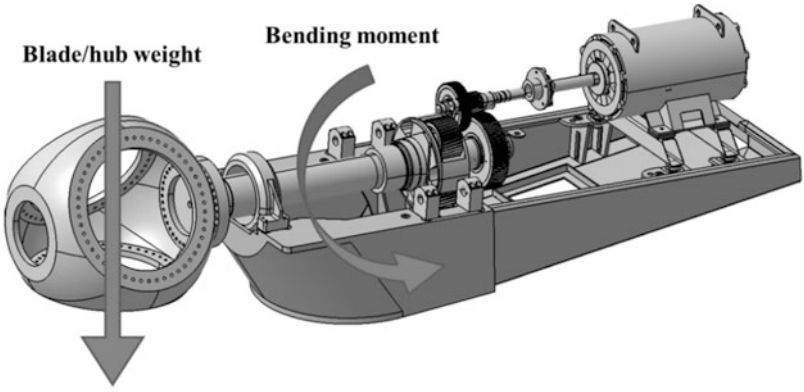

Fig. 9.4 Non-torque loadings and their effects on a typical 3-point suspension drivetrain

The shaft pitching moment causes unequal load sharing between the upwind and downwind planet bearings, which can lead to abnormal tooth contact (consisting of tooth-edge loading, partial contact loss and reversing contact). These conditions can result in tooth failure modes such as micro-pitting. At low-input torque, the effects of non-torque loads on the gearbox internal loads were dominant. In this condition, the planet bearings are at risk of skidding and the gear teeth are at risk of contact loss, also leading to reduced gearbox life. The planetary load-sharing factor increased with bearing clearance. With carrier bearing-clearance, the shaft pitching moment was transmitted into the gear meshes and planet bearings. Optimizing the carrier-bearing clearance reduced the gearbox sensitivity to non-torque loads.

9.3 Numerical Modelling of Bearings

Modelling and simulation methods provide an increasingly accurate approach for predicting the dynamic performance of mechanical systems. The bearing models evolved from analytical formulations of a nonlinear spring to complex flexible multibody simulations. An overview of these modelling approaches is given in Sect. 9.3.1, while the technical details of the various approaches are discussed in Sects. 9.3.2–9.3.4.

9.3.1 Overview of State-of-the-Art Bearing Models

A bearing is a mechanical component that constraints the relative motion between two bodies by allowing relative rotation about one axis and constraining relative motion along the other coordinates (i.e. two relative rotations and three relative translational displacements). Due to the finite stiffness of a mechanical bearing and the presence of clearance, however, relative motion along the constrained coordinates can occur in practice when the bearing deforms or moves through its clearance. As such, a mechanical bearing can be viewed as a multi-dimensional spring with non-linear (state-dependent) stiffness constants. In this representation, the non-linearity of the spring is caused by clearance, the varying number of rolling elements in contact and the nonlinear nature of these contact interactions (see Sect. 9.2.2).

The representation of a mechanical bearing as a multi-dimensional spring has proven to be a productive ground for modelling bearings in modal analyses of multibody systems (Peeters 2006; Helsen 2012). As such analyses are typically conducted at a (or a sequence of) predefined operating point(s) of the multibody system, the non-linear bearing can be linearized and represented by a three-dimensional linear spring. This spring is mathematically described by a constant symmetric 6-by-6 stiffness matrix (typically provided by the bearing manufacturer), which represents the relationship between the relative motion of the bearing's inner

and outer rings and the resulting bearing forces. However, as this representation is only valid at a specific operating point, it cannot be used for time domain simulations when the nonlinear bearing stiffness and/or internal bearing dynamics are expected to play an important role in explaining the overall system behavior. In the latter case, non-linear bearing models should be used.

A first distinction in non-linear bearing modelling is based on the dimensionality of the problem: if only in-plane motion is considered, two-dimensional bearing models are to be used. These models allow relative rotation about the axis perpendicular to the plane, while constraining translational motion in the plane (note that for modal analyses, a linearized 2D bearing model represented by a 3-by-3 stiffness matrix usually suffices). Three-dimensional bearing models are used when general motion is considered; in this case two relative rotations and three relative translations are constrained by the bearing model. Two-dimensional bearing models are discussed in Sect. 9.3.2, whereas three-dimensional models are discussed in Sect. 9.3.3.

A second distinction is based on the level of complexity and detail included in the flexibility description of the bearing. In Sects. 9.3.2–9.3.3, it is assumed that the (elastic) deformation of the bearing is confined to the contact zones within the bearing (i.e. the areas over which contact takes place between the rolling elements and the inner and outer raceways). Under this assumption, Hertzian contact theory (cf. Sect. 9.2.2) suffices to describe the elastic deformation of the bearing and to compute bearing stiffness. While the assumption of localized deformation is reasonable in a wide range of applications as far as the (generally compact and solid) rolling elements are concerned, this might not be the case for the bearing's inner and/or outer rings, especially when they are integrated with the bearing's flexible supporting structure (e.g. gearbox housing). In that case, Hertzian contact theory only describes the local contribution to the overall bearing deformation, whereas more advanced methods are required to describe the global (or 'bulk') bearing deformation. Such methods are described in Sect. 9.3.4.

Further distinctions of the various bearing models are based on the following aspects:

- **Type of bearing**: typically, a distinction is made between ball bearings (point contact between rolling elements and raceways) and roller bearings (line contact between rolling elements and raceways), because of the different mathematical tools required to model the contact interactions.
- Inclusion of **dynamic effects** such as centrifugal, gyroscopic and inertial effects: these effects can either be taken into account quasi-statically (excluding inertial effects) or by assigning a dynamic degree of freedom to each rolling element in the bearing model. In quasi-static bearing models the solution to a set of nonlinear algebraic equilibrium equations is generally required, while in dynamic models the solution is obtained through integration of the differential equations of motion of the bearing elements. Obviously, the importance of dynamic effects increases as the bearing's cage velocity increases.

- Inclusion of the influence of **elasto-hydrodynamic lubrication** (EHL): lubrication reduces friction and wear in the contact interactions between rolling elements and raceways. The stiffness and damping properties of the EHL film play an important role in the transfer of mechanical vibrations through the bearing, and should therefore be taken into account when investigating internal bearing dynamics. As damping in the EHL film is mainly attributed to viscous losses in the lubricant (Wensing 1998), the damping behavior of the lubricant is typically taken into account by adding a linear viscous damper in parallel with the nonlinear contact stiffness spring. Wijnant (1998) obtained an analytical expression for the EHL damping constant in ball bearings by solving (for various parameters) the structural and fluid equations governing the transient behavior of a single EHL contact in which an initially equilibrated rolling element is slightly lifted from its equilibrium position and subsequently released. Similar analyses have been conducted for roller bearings (Qian 2013). Furthermore, the stiffness of a fully-developed lubricant film generally is several orders of magnitude larger than the Hertzian contact stiffness and therefore its contribution to the flexibility of the contact zone can be neglected.
- Inclusion of the **cage**: the rolling elements are usually held in an angularly spaced relationship by a cage or separator, which is generally constructed using materials that are relatively soft as compared to the rolling element and ring materials. A properly designed cage is often crucial for the bearing to withstand misalignment loads, and can therefore play an important role in establishing equilibrium of the bearing components. Cage modelling varies from (implicitly defined) geometric constraint relations to the inclusion of flexible cage representations including contact modelling of the interactions between cage and rolling elements.
- Inclusion of the influence of **friction**: friction in a bearing is made up of several components, including rolling friction, sliding friction of both the rolling elements and the cage, fluid friction and seal friction. These components lead to (motion-resisting) frictional forces and moments in the bearing that can modify the equilibrium conditions in the bearing. Friction energy is converted to heat, which is mostly dissipated by the (preferably recirculating) lubricant. Friction in particular plays a role in cylindrical and tapered roller bearings, where sliding contact between the roller ends and ring flanges can result in considerable frictional forces.

In the subsequent sections, the focus will be on dry (i.e. non-lubricated) frictionless contact between the rolling elements and raceways. One of the main complexities in developing a non-linear bearing model is determining the mutual approach between a rolling element and a raceway, which generally requires a thorough geometrical analysis of the bearing. Once an expression for the mutual approach is obtained, its derivative with respect to time can be computed relatively easily (if not analytically, then using finite differencing) and this information can potentially be used to include the effect of EHL damping in the model by including a linear viscous damper. Finally, frictional forces are assumed to only slightly alter the load distribution across the rolling elements and will therefore not be considered in

the present work (the interested reader is referred to Gupta (2012) for the inclusion of frictional forces and moments in the bearing model).

9.3.2 Two-Dimensional Bearing Models

2D bearing models are typically used when investigating the global dynamical behavior of a planar multibody system (or one that can be idealized as such), or when the axial forces and misalignment torques (i.e. torques about the in-plane axes) in the bearing are negligible. Most two-dimensional bearing models in literature are based on (all of) the following assumptions:

- The rolling elements and inner and outer rings have motions in the plane of the bearing only;
- All deformations occur according to the Hertzian theory of elasticity, plastic deformations are neglected, and there is no bulk deformation of the bearing's components;
- The cage ensures a constant angular separation between rolling elements, hence there is no interaction between the rolling elements;
- There is no slipping of the rolling elements as they roll over the raceways;
- The bearings are assumed to operate under isothermal conditions such that thermal effects like the expansion of rolling elements and raceways and the change of lubricant viscosity can be neglected.

The assumptions of two-dimensional bearing modelling most naturally apply to bearings that are characterized by point contacts, such as ball bearings. Nevertheless, two-dimensional models have been used to model roller bearings as well, with only minor changes to the mathematical framework, as discussed below.

One of the distinguishing features of the various planar bearing models is the way the contact interactions and the inertial properties of the rolling elements are modelled. In a static bearing model (Fig. 9.5a), each rolling element (and the contact

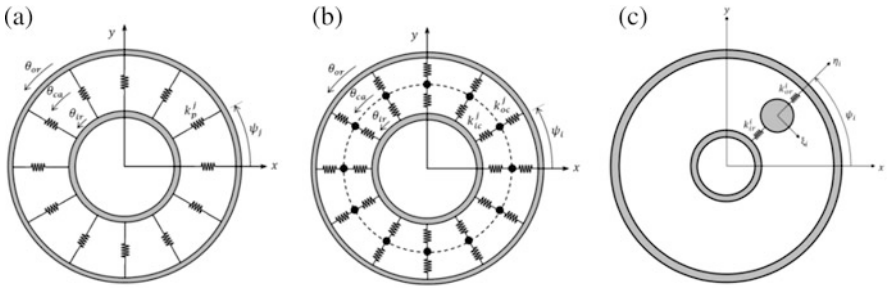

Fig. 9.5 2D bearing models: (**a**) static bearing model, (**b**) quasi-static bearing model, (**c**) dynamic bearing model

interactions it has with both the inner and outer raceways) is represented by a single non-linear spring having zero stiffness when the spring is stretched. In this case, all dynamic effects that are due to the motion of the rolling elements (i.e. inertial and centrifugal forces) are neglected. Centrifugal effects are taken into account by the quasi-static bearing model (Fig. 9.5b) where each contact interaction is represented by a non-linear spring (i.e. two springs in series for each rolling element), and a centrifugal force proportional to the cage's angular velocity is applied at the interconnection between the two springs. This force acts to increase the clearance between the inner raceway and the rolling elements, and therefore alters the contact forces applied to the respective raceways (which are equal in magnitude in the case of the static bearing model). In addition to the series arrangement of non-linear springs, the dynamic bearing model (Fig. 9.5c) takes into account the mass of each rolling element and adds one degree of freedom per rolling element to the bearing's equations of motion. The latter are typically obtained by substituting the bearing's kinetic and potential energies into Lagrange's equation of motion, and need to be integrated in time simultaneously with the equations governing the dynamic behavior of the remainder of the multibody system.

Irrespective of the type of bearing model that is used, one critical aspect of modelling bearings, both in planar and spatial modelling, is the computation of the contact stiffness of the interaction between a rolling element and a raceway. The contact stiffness appears in the load-displacement relationship of the contact interaction, which has the form of the power law $Q = K_c \delta^p$, where Q is the contact load, K_c is the contact stiffness, δ is the mutual approach between rolling element and raceway, and p is the exponent—the latter is equal to 3/2 for point contacts according to Hertz's theory and is usually taken to be 10/9 in the case of line contact (de Mul et al. 1989b). The contact stiffness K_c depends on the contact geometry (radii of curvature of the contact surfaces) and the material properties (Young's modulus and Poisson's coefficient), and closed-form expressions are readily available in e.g. Harris and Kotzalas (2006). Because of the different geometries of the inner and outer raceways, the raceways typically have different contact stiffnesses.

Technical details on the mathematical derivation and implementation of two-dimensional bearing models are readily available in literature. Static bearing models including the effects of non-linear contact stiffness, varying number of rolling elements in contact and radial clearance were used in Abbes et al. (2011), Kappaganthu and Nataraj (2011), and Xu and Li (2012) to study the dynamic behavior of respectively a pair of helical gears supported by ball bearings, a rotor-bearing system and a slider-crank including a ball bearing joint. The inclusion of centrifugal effects in quasi-static bearing models is discussed in Hamrock and Anderson (1983), which includes a comprehensive overview of bearing modelling and all related aspects. Furthermore, an investigation of the influence of centrifugal effects is included in Liew et al. (2001). Dynamical two-dimensional ball bearing models were used in Harsha (2005) and Dougdag et al. (2012) to investigate the influence of bearing defects on system dynamics. Leblanc et al. (2009) developed

a dynamical two-dimensional roller bearing including the influence of EHL and contact interactions with the cage.

9.3.3 Three-Dimensional Bearing Models

3D bearing models offer far greater insight into the internal bearing dynamics than their two-dimensional counterparts. They are typically used when the dynamic performance of the bearings are at the heart of the investigation, or when a three-dimensional bearing representation is necessary to accurately grasp the global system behavior, e.g. when axial forces and/or misalignment torques are expected to play an important role. While compared to the overall computational cost of general multibody systems the three-dimensional bearing models are not significantly less efficient than the 2D models, the numerical implementation of these models is often considerably more involved. Due to the fundamental differences in the nature of the contact interactions (point vs. line contact), different mathematical models are typically used to model ball and roller bearings.

9.3.3.1 Ball Bearings

In the case of point contacts, all internal bearing forces and moments originate from simple Hertzian point contact interactions (between rolling elements and raceways) that are described by the same load-displacement relationship given in Sect. 9.3.2. The complexity of three-dimensional ball bearing models is therefore solely related to the rather complex geometry and kinematics of three-dimensional ball bearings.

The first to investigate three-dimensional ball bearing models in a systematic way was Jones (1960). He formulated a quasi-static three-dimensional ball bearing model that included the influence of centrifugal forces and gyroscopic moments. The model consists of five nonlinear, simultaneous equilibrium equations (corresponding to the five coordinates that are constrained by the bearing, cf. Sect. 9.3.1) that need to be linearized and solved iteratively by the Newton-Raphson method. The complexity of the model lies mainly in determining the internal bearing forces and moments, which are expressed w.r.t. a reference frame that is aligned with the shaft (or bearing inner ring), leading to rather cumbersome expressions, especially when the influence of quadratic velocity terms is included.

In response to the complexity of the Jones model, Gupta (2012) developed a dynamical ball bearing model (in which each ball bearing was assigned with a number of degrees of freedom), arguing that despite the increased computing effort in obtaining a solution (through integration of the equations of motion), the dynamic model provides a significant reduction in the overall design costs of the model (as the influence of centrifugal and gyroscopic effects follows naturally from the bearing's equation of motion). Furthermore, the dynamic model is free of the typical convergence problems that are associated with solving equilibrium solutions

in quasi-static bearing models, and therefore are better suited for including lubricant behavior (Gupta 2012).

Another simplification of the model of Jones was provided by de Mul et al. (1989a), who developed a quasi-static bearing model in five degrees of freedom and including centrifugal forces. The formulation of the model is less cumbersome than the model of Jones and lends itself better for computer implementation. Assuming no circumferential motion of the rolling element at equilibrium, the equilibrium equations for each roller element are formulated in a plane (two translations and one rotation) at the rolling element level, and are then transformed to the central bearing reference frame through a 3-by-5 transformation matrix. The mutual approach between rolling element and raceway is obtained through a comparatively simple two-dimensional geometric analysis, and closed-form expressions for the bearing's global stiffness matrix are provided.

9.3.3.2 Roller Bearings

The classical Hertzian theory is usually not valid for roller contact. This can be either because of the dimension of the contact area that exceeds the assumption of Hertz, due to noncircular contact profiles, or due to high loads making the contact ellipse being truncated at the end of the rollers. These types of problems are referred to as non-Hertzian contact problems and there is, unfortunately, no exact and explicit relationship available for expressing the load as a function of the deflection. Many authors, such as Lundberg and Sjövall (1958), Palmgren (1959), and Young and Budynas (2002), have addressed these types of problems based on half-space theory and experiments to find an, often implicit, relationship between the load and the deformation. These relationships are often found in idealized contact situations (e.g. no misalignments, close to half-space conditions) and sometimes even profiled roller geometries.

More recently, numerical techniques are adopted to account e.g. for misaligned rollers. Some authors numerically integrate the Boussinesq's half-space theory to iteratively obtain the required solution (Reusner 1977; Andréason 1973). Others apply more simple techniques (Harris and Kotzalas 2006; Andréason 1973), however less accurate, for computational reasons in case that multiple contacts need to be solved simultaneously. In the so-called slicing technique, the contact length is sliced into a number of laminae. Each slice is given a fraction of the total roller stiffness, which is often based on some of the above mentioned load-deflection relations. A distinction can be made in whether each slice is treated separately, and thus having no effect on the deflection of adjacent slices, or treated in a combined way, and thus having a mutual influence. In the former case, pressure concentrations cannot be taken into account. Nevertheless, the problem is less expensive to solve. In the other case, where the deflection of one slices depends on the deflection of other slices, iterative procedures are required. Teutsch and Sauer (2004) propose a method in which the optimum between accuracy and efficiency is searched for.

The modelling of 3D roller bearings is conceptually similar to ball bearings; the mutual approach between the contacting bodies has to be found such that the load-deflection relation can be applied and the contact forces computed. As mentioned above, the slicing technique is often used to discretize the roller into a set of laminae. Consequently, the mutual approach of each slice to the bearing raceway should be determined by a (kinematic) model.

As for ball bearings, many authors have provided various levels of complexity. Gupta (2012) followed his own approach for ball bearings and assigned again degrees-of-freedom to the rollers. The slicing technique is adopted to compute the roller contact forces. In models such as those of de Mul et al. (1989b) and Andréason (1973), among many others, the equilibrium equations are again determined in a two-dimensional plane at rolling element level and include the centrifugal and gyroscopic forces in a quasi-static way. de Mul et al. (1989b) refer next to the slicing technique also to a more sophisticated technique to model non-Hertzian contact in a general way that was presented in de Mul et al. (1986).

To end this section, it should be noted that rollers are profiled by the bearing manufacturers, in order to optimize the stress distribution over the rollers for a particular loading condition and to avoid high edge stresses that can substantially exceed the computed stresses in case of separately treated slices. The knowledge of the profile, as for the geometry of the raceways and rolling elements in bearings, is key for an accurate prediction of the contact stresses and the stiffness of a bearing.

9.3.4 Bearings with Distributed Flexibility

The above listed solutions pertain to bearings that have rigidly supported rings. The considered deflections are the local Hertzian deformations and are based on the assumptions presented in 9.2.2. In some applications, however, the influence of the supporting structure's and ring's flexibility can be decisive for the bearing's behavior as it might affect, for instance, the load distribution over the rolling elements. Consequently, the global (or bulk) deformations such as the bending of the bearing housing cannot always be neglected.

An obvious way to tackle this modelling problem is to use the *Finite Element* (FE) method to include and combine both the local nonlinear contact deflections and the global flexibility of the ring and supporting structure. In addition, the influence of e.g. materials, manufacturing errors, lubrication, and cage effects has been investigated by adding those effects to (nonlinear) FE codes. A brief overview of such codes is given in Qian (2013). Although these (nonlinear) FE approaches have proven their value for many high technology applications, they suffer from some severe disadvantages for drivetrain modelling. First, since the contact interaction (or mutual approach) between the rolling elements and the raceways can generally not be sought purely analytically as for the techniques listed in the previous sections, some standard contact detection algorithms are obliged to search for contact in all possible contact elements. This process is often the most time-consuming process

in dynamic contact simulations. It should however be mentioned that, generally, the known (undeformed) geometry can in fact be exploited to reduce the number of possible contact elements for a specific rolling element. A second disadvantage is that one has to rely on FE models with a highly refined mesh at the contact zone and thus a large number of nodes in order to capture the nonlinear behavior of the Hertzian contact with a reasonable accuracy. The resulting models have therefore an extremely high number of *degrees-of-freedom* (DOFs). For time-domain analyses of gearboxes and drivetrains, where it is not uncommon to have multiple bearings and gears, these models result in unacceptable simulation times.

Model order reduction schemes can be introduced to lower the dimensionality of the problem to alleviate above mentioned computational burden with a minimal loss of accuracy. However, traditional model order reduction techniques typically become inefficient for models with time-varying load locations, as is the case for the moving rolling elements in a bearing. In fact, to obtain a favorable accuracy on displacement and stress levels one has to include so-called static modes for each of the interacting nodes in the reduction space, as it is likely that almost every node positioned on the raceway of the bearing can be loaded by the rolling elements. This action might result in a poor reduction in terms of DOFs.

To deal with the latter problem, some advanced model order reduction techniques have been developed to accurately simulate problems with time-varying load locations, such as gears and bearings. A statically complete procedure is provided by the *Static Modes Switching* (SMS) method (Heirman et al. 2011), which has been applied to the gear contact problem in Tamarozzi et al. (2013). SMS makes use of a discontinuously changing reduction basis, of minimal dimension, by taking advantage of the fact that each time step only a few out of many interface DOFs are loaded simultaneously. The technique has been modified in Tamarozzi et al. (2014) to obtain a continuously time-varying reduction space by use of a parametric relationship describing the location of externally applied moving loads, further referred to as *Static Mode Sliding* (SMS^2). It has been shown that the price to pay for the very compact reduction basis is the evaluation of some extra terms in the equations of motion. This model order reduction strategy is later extended and applied for the simulation and prediction of the behavior of an indirect dynamic bearing force measurement setup (Fiszer et al. 2015b) and for efficient time-simulation of gear pairs (Blockmans et al. 2015). In Blockmans et al. (2015), the performance of the novel technique is demonstrated by simulating a dynamic gear contact problem and comparing results against traditional model reduction techniques as well as commercial nonlinear finite element software.

Although the computational burden is alleviated by use of the model order reduction techniques, a highly refined mesh at the contact zone is still required to capture the nonlinear behavior of the Hertzian contact. The latter retains the need for a large number of so-called static modes to be computed in a pre-processing step, despite the fact that only few are active at a certain moment in time during the simulation.

Some authors have proposed to combine analytic solutions with the FE method, (Wensing 1998; Andersson and Vedmar 2003; Vijayakar 1991; Fiszer et al. 2015a), thereby eliminating the need for highly refined meshes at the contact zone. The main advantage of such a semi-analytic strategy lies in the accurate contact description that combines the nonlinear effects present at the contacting interface with a standard FE formulation in those regions in which nonlinear effects are not prominent. Therefore, coarser FE meshes can be used; these meshes should only accurately represent the more global bulk deformation.

In the semi-analytic strategy presented by Wensing (1998), the total deformation is separated in the bulk deformation, represented by a reduced order model, and the nonlinear local Hertzian deflections at the contact zone. The multitude of static shape vectors is replaced by a comparatively small set of global constraint modes to capture the effect of the bulk flexibility of the rings, supporting structure and the mounting conditions on the behavior of the bearings. The global constraint modes are determined by use of Chebyshev polynomials, which are also utilized as contact geometry. These analytic surfaces are then used to determine the mutual approach between the ring and the rolling element to compute the contact forces based on Hertzian contact theory.

The approach presented in Fiszer et al. (2015a) offers an equivalent semi-analytic strategy. Nevertheless, the global constraint modes, that are used to reduce the FE model representing the bulk deformation, are replaced by global attachment modes. The latter allows for a one-to-one relation between the contact load and the static mode, such that a parametric relationship describing the contact location can be defined and the efficient model reduction technique SMS^2 becomes applicable. In addition, the Chebyshev polynomials that represent smooth interacting raceways are replaced by NURBS or B-spline surfaces. It is shown in Fiszer et al. (2015b) that by selecting an appropriate basis for the B-splines, the interacting surface can be composed by a linear combination of the control points, using the modal participation factors (or reduced elastic coordinates) of the affected mode shapes during simulations. These offline computed B-splines or NURBS are therefore referred to as NURBS-modes.

9.4 Conclusions: Towards Unified Wind Turbine Gearbox Models

Sections 9.2 and 9.3 underlined some key aspects regarding the behavior and the modelling of wind turbine drivetrains with a specific focus on bearings. It goes without saying that another major component that needs to be accurately simulated within drivetrains, are gears. Helical stages and planetary helical stages are mostly of relevance in this framework. Similarly to bearings, gears are also complex components in which accurate geometry, material properties and lubrication play an important role. They can also be simulated with different levels of complexity

ranging from analytical models and lumped parameter models (Özgüven and Houser 1988; Cai and Hayashi 1994; Kuang and Yang 1992; Velex 2012; Kahraman 1993; Eritenel and Parker 2012; Kahraman 1994; Lin and Parker 1999; Andersson and Vedmar 2003) up to fully flexible non-linear contact simulations (Tamarozzi et al. 2013; Blockmans et al. 2015; Ziegler et al. 2006; Parker et al. 2000). The literature about gear modelling and analysis is as rich as the one for bearings and it is out of the scope of this chapter to provide a detailed review.

While the modelling of single components can be interesting for troubleshooting of localized problems in a wind turbine gearbox, these are seldom enough to draw conclusions regarding the behavior of the full drivetrain. In order to benefit from the different levels of complexity in which gears and bearings can be represented, there is a strong need for coupling them to system-level simulation tools such as e.g. multibody and flexible multibody models. Multibody simulation is an established technology that is aimed to investigate the dynamic behavior of systems of interconnected bodies. Within this type of models it is possible to connect different body representations (e.g. rigid or flexible) by making use of idealized joints or force elements that can represent localized stiffness and damping with different levels of complexity. Examples of wind turbine drivetrains modelled through multibody simulation can be found in Helsen (2012) and Vanhollebeke (2015).

Multibody models with idealized joints or constraints form a set of highly non-linear Differential Algebraic Equations (DAE). For relatively simple systems with mainly rigid bodies, computational strategies exist to perform dynamic transient simulations in a relatively short time-frame. Depending on the phenomena that need to be investigated, bearings and gears models can be included in multibody models with different levels of complexity. In order to achieve drivetrain models that are of wide applicability and address different design questions some research effort still needs to be focused on several open topics as e.g.:

- *Scalability of different model complexities* for bearings and gears to be included in system level simulation. In particular bearings and gears can be idealized in different ways but all the different model types should be able to interact with their surrounding environment. Depending on the model complexity adopted for the different components, these interactions can happen at localized or distributed interfaces. As an example, a gear or a bearing can be modelled in three dimensions as a 6×6 stiffness matrix that interacts with shafts and housing through forces and torques acting at localized interface points. On the other extreme, flexible gear models and bearings interact with their surrounding structure through distributed FE interface nodes. The inherently different interface behavior of the modelling strategies makes it difficult to create a single drivetrain model that is scalable for different levels of complexity depending on the target use. The inclusion of 3D modelling capabilities within natively 1D environments such as Matlab Simulink, SISW Imagine. Lab Amesim, Dymola, etc.... could potentially alleviate these difficulties and is topic of current research.

- Advanced drivetrain models including e.g. flexible housing deformation, contact mechanics models for gears and bearings, spline connection models, etc.... can easily become computationally cumbersome. Modern linear and non-linear model order reduction techniques are one of the main research fields from which wind turbine drivetrain modelling could benefit.

Sections 9.1–9.3 summarized a few key focal points regarding drivetrain modelling in a wind turbine context with specific focus on state-of-the-art of bearing modelling. The discussion should not be considered as exhaustive but underlines a few important items to be considered when analyzing and simulating drivetrains. The improvements of components modelling methods (e.g. bearing and gears) and scalable inclusion in system-level simulation tools for accurate and affordable drivetrain analysis remain (partially) open challenges where further research efforts needs to be focused.

Acknowledgements The authors would like to gratefully acknowledge the European Commission for their support of the MAREWINT research project (GA 309395). Additionally, the IWT Flanders within the OPTIWIND project and the Research Fund KU Leuven for the IDO_WIND project are kindly acknowledged for their support.

References

Abbes MS, Hentati T, Maatar M et al (2011) Dynamic analysis of helical gears supported by rolling elements bearings. J Theor Appl Mech 41(1):33–50

Andréason S (1973) Load distribution in a taper roller bearing arrangement considering misalignment. Tribology 6(3):84–92. doi:10.1016/0041-2678(73)90241-8

Andersson A, Vedmar L (2003) A dynamic model to determine vibrations in involute helical gears. J Sound Vib 260(2):195–212

Blockmans B, Tamarozzi T, Naets F et al (2015) A nonlinear parametric model reduction method for efficient gear contact simulations. Int J Numer Methods Eng 102(5):1162–1191

Brandlein J, Eschmann P, Hasbargen L et al (1999) Ball and roller bearings: theory, design and application. Wiley, Chichester

Cai Y, Hayashi T (1994) The linear approximated equation of vibration of a pair of spur gears (theory and experiment). J Mech Des 116(2):558–564

Chen W, Alewine K (2010) Wind turbine generator failure modes analysis and occurrence. Paper presented at the Wind Power, Dallas, 24–26 May 2010

de Mul JM, Kalker JJ, Fredriksson B (1986) The contact between arbitrarily curved bodies of finite dimensions. J Tribol 108(1):140–148
de Mul JM, Vree JM, Maas DA (1989a) Equilibrium and associated load distribution in ball and roller bearings loaded in five degrees of freedom while neglecting friction – part I: general theory and application to ball bearings. J Tribol 111(1):142–148
de Mul JM, Vree JM, Maas DA (1989b) Equilibrium and associated load distribution in ball and roller bearings loaded in five degrees of freedom while neglecting friction – part II: application to roller bearings & experimental verification. J Tribol 111(1):149–155
Dietl P, Wensing J, van Nijen G (2000) Rolling bearing damping for dynamic analysis of multibody systems: experimental and theoretical results. Proc Inst Mech Eng K J Multi-Body Dyn 214:33–43
Dougdag M, Ouali M, Boucherit H et al (2012) An experimental testing of a simplified model of a ball bearing: stiffness calculation and defect simulation. Meccanica 47(2):335–354
Eritenel T, Parker RG (2012) Three-dimensional nonlinear vibration of gear pairs. J Sound Vib 331(15):3628–3648
EWEA (2011) Upwind: design limits and solutions for very large wind turbines. In: European Wind Energy Association Wind Energy Association Reports. Available via EWEA. http://www.ewea.org/fileadmin/files/library/publications/reports/UpWind_Report.pdf. Accessed 08 Apr 2016
Fiszer J, Tamarozzi T, Desmet W (2015a) A semi-analytic strategy for the system-level modelling of flexibly supported ball bearings. Meccanica. doi:10.1007/s11012-015-0318-6
Fiszer J, Tamarozzi T, Blockmans B et al (2015b) A time-dependent parametric model order reduction technique for modelling indirect bearing force measurements. Mech Mach Theory 83:152–174
Gegner J (2011) Tribological Aspects of Rolling Bearing Failures. In: Kuo CH (ed) Tribology – lubricants and lubrication. InTech, Rijeka, pp 33–94
Grubin A (1949) Fundamentals of the hydrodynamic theory of lubrification of heavily loaded cylindrical surfaces. In: Ketova KhF (ed) Symposium on Investigation of the Contact of Machine Components, Moscow, 1949, Central Scientific Research Institute for Technology and Mechanical Engineering, vol 30. TsNIITMASh, Moscow, p 115
Guo Y, Keller J, LaCava W (2014) Planetary gear load sharing of wind turbine drivetrains subjected to non-torque loads. Wind Energy 18(4):757–768
Gupta PK (2012) Advanced dynamics of rolling elements. Springer, New York
Hamrock BJ, Anderson WJ (1983) Rolling-element bearings. NASA Reference Publication 1105. National Aeronautics and Space Administration Publications. Available via NASA NTRS. http://ntrs.nasa.gov/archive/nasa/casi.ntrs.nasa.gov/19830018943.pdf. Accessed 08 Apr 2016
Harris TA, Kotzalas M (2006) Advanced concepts of bearing technology: rolling bearings analysis. Taylor and Francis, New York
Harsha SP (2005) Non-linear dynamic response of a balanced rotor supported on rolling element bearings. Mech Syst Signal Process 19(3):551–578
Heirman GHK, Tamarozzi T, Desmet W (2011) Static modes switching for more efficient flexible multibody simulation. Int J Numer Methods Eng 87(11):1025–1045
Helsen J (2012) The dynamics of high power density gear units with focus on the wind turbine application. Dissertation, KU Leuven
ISO (2007) ISO 281:2007 Rolling bearings – dynamic load ratings and rating life. ISO, Geneva
Jacobs W (2014) Experimental analysis of the dynamic characteristics and lubricant film of a ball bearing under combined static and dynamic load. Dissertation, KU Leuven
Jones AB (1946) New departure engineering data; analysis of stresses and deflections. Bristol Conn, New Departure, Division General Motors Corp, Chicago
Jones AB (1960) A general theory for elastically constrained ball and radial roller bearings under arbitrary load and speed conditions. J Basic Eng 82(2):309–320
Kahraman A (1993) Effect of axial vibrations on the dynamics of a helical gear pair. J Vib Acoust 115(1):33–39
Kahraman A (1994) Planetary gear train dynamics. J Mech Design 116(3):713–720

Kappaganthu K, Nataraj C (2011) Nonlinear modeling and analysis of a rolling element bearing with a clearance. Commun Nonlinear Sci 16(10):4134–4145

Kuang JH, Yang YT (1992) An estimate of mesh stiffness and load sharing ratio of a spur gear pair. In: The 1992 ASME design technical conferences – 6th international power transmission and gearing conference, Scottsdale, September 1992. Advancing Power Transmission into the 21st Century, vol 1. ASME, New York, p 1

Leblanc A, Nelias D, Defaye C (2009) Nonlinear dynamic analysis of cylindrical roller bearing with flexible rings. J Sound Vib 325(1):145–160

Li Y, Billington S, Kurfess C et al (1999) Adaptive prognostics for rolling element bearing condition. Mech Syst Signal Process 13(1):103–113

Liew A, Feng NS, Hahn EJ (2001) Transient rotordynamic modeling of rolling element bearing systems. In: Abstracts of the ASME Turbo Expo 2001: Power for Land, Sea, and Air, American Society of Mechanical Engineers, New Orleans, 4–7 June 2001

Lin J, Parker RG (1999) Analytical characterization of the unique properties of planetary gear free vibration. J Vib Acoust 121(3):316–321

Lundberg G, Sjövall H (1958) Stress and deformation in elastic contacts. Institution of Theory of Elasticity and Strength of Materials, Gothenburg

Mitsuya Y, Sawai H, Shimizu M, Aono Y (1998) Damping in vibration transfer through deepgroove ball bearing. J Tribol 120:413–420

Muro H, Tsushima N (1970) Microstructural, microhardness and residual stress changes due to rolling contact. Wear 15:309–330

Nierlich W, Gegner J (2011) Material response bearing testing under vibration loading. In: Beswick J (ed) Selected Technical Papers STP 1548 Bearing Steel Technologies. Ninth International Symposium on Bearing Steel Technologies, November 2011. Advances in Rolling Contact Fatigue Strength Testing and Related Substitute Technologies, vol 9. ASTM, New York

Nonato F, Cavalca K (2012) Local linear approximation for the stiffness characteristics of elastohydrodynamic point contacts. In: Abstracts of the 10th international conference on vibrations in rotating machinery, IMechE, London, 11–13 Sep 2012

Özgüven HN, Houser DR (1988) Mathematical models used in gear dynamics–a review. J Sound Vib 121(3):383–411

Palmgren A (1959) Ball and roller bearing engineering. SH Burbank, Philadelphia

Park YJ, Lee GH, Song JS, Nam YY (2013) Characteristic analysis of wind turbine gearbox considering non-torque loading. J Mech Des 135(4):044501–044508. doi:10.1115/1.4023590

Parker RG, Agashe V, Vijayakar SM (2000) Dynamic response of a planetary gear system using a finite element/contact mechanics model. J Mech Des 122(3):304–310

Peeters J (2006) Simulation of dynamic drive train loads in a wind turbine. Dissertation, KU Leuven

Qian W (2013) Dynamic simulation of cylindrical roller bearings. Dissertation, RWTH Aachen University

Reusner H (1977) Druckflächenbelastung und Oberflächenverschiebung im Wälzkontakt von Rotationskörpern. Dissertation TH Karlsruhe

Tamarozzi T, Ziegler P, Eberhard P et al (2013) Static modes switching in gear contact simulation. Mech Mach Theory 62:69–106. doi:10.1016/j.mechmachtheory.2013.01.006

Tamarozzi T, Heirman GH, Desmet W (2014) An on-line time dependent parametric model order reduction scheme with focus on dynamic stress recovery. Comput Methods Appl Mech Eng 268:336–358

Teutsch R, Sauer B (2004) An alternative slicing technique to consider pressure concentrations in non-Hertzian line contacts. J Tribol 126(3):436–442

Vanhollebeke F (2015) Dynamic analysis of a wind turbine gearbox: towards prediction of mechanical tonalities. Dissertation, KU Leuven

Velex P (2012) On the modelling of spur and helical gear dynamic behaviour. Cornell University Library: Classical Physics. Available via arXiv. http://arxiv.org/pdf/1204.2636v1 preprint arXiv:1204.2636. Accessed 07 Apr 2016

Vijayakar S (1991) A combined surface integral and finite element solution for a three-dimensional contact problem. Int J Numer Methods Eng 31(3):525–545
Wensing J (1998) On the dynamics of ball bearings. Dissertation, University of Twente
Wijnant Y (1998) Contact dynamics in the field of elastohydrodynamic lubrication. Dissertation, University of Twente
Xu LX, Li YG (2012) An approach for calculating the dynamic load of deep groove ball bearing joints in planar multibody systems. Nonlinear Dyn 70(3):2145–2161
Young WC, Budynas RG (2002) Roark's formulas for stress and strain, vol 7. McGraw-Hill, New York
Ziegler P, Eberhard P, Schweizer B (2006) Simulation of impacts in geartrains using different approaches. Arch Appl Mech 76:537–548
Zwirlein O, Schlicht H (1980) Werkstoffanstrengung bei Wälzbeanspruchung - Einfluss von Reibung und Eigenspannungen. Werkstofftechnik 1:11–14

Chapter 10
Experimental Characterization of Wind Turbine Gearbox in Operation

Emilio Di Lorenzo and Simone Manzato

Abstract The gearbox is one of the key subsystems in a geared wind turbine, as it must transfer the power from the low speed shaft connected to the rotor to the high speed shaft connected to the generator. As turbines become larger, more power can be generated, but consequently gearboxes with higher load capacity need to be designed. Gaining a deep knowledge into gearbox dynamics becomes of fundamental importance and more and more accurate and detailed noise and vibration measurements are demanded. When dealing with a machine in operating conditions with several rotating components and, in particular with a multi-stage transmission system, components are introduced in the signal that make the application of standard techniques such as Operational Modal Analysis (OMA) very difficult and in some cases almost impossible. For this reason, new techniques to tackle with these conditions have been investigated, such as Order Based Modal Analysis (OBMA). As suggested by its own name, this technique is a combination of Order Tracking and Operational Modal Analysis. On one hand, OMA is based upon the calculation of auto- and cross-powers and it works very well for most cases. On the other hand, OBMA is based upon the extracted orders during run-up or coast-down. During such events, the orders are sweeping through a certain frequency band which is useful for characterizing the dynamic behavior of the rotating structures.

10.1 Introduction and Motivation

The current approach in industry is to qualitatively measure the vibrations generated by the dominant excitation sources as well as the overall sound power levels, so that the machine performance can be certified according to standards and/or customer specifications. However, as mentioned, by following this approach only qualitative information can be obtained and the root causes of high vibration levels or acoustic tonalities cannot be understood. Also, analyzing these data requires a lot of user-interaction, as each peak need to be independently analyzed. Experimental modal analysis techniques (Heylen et al. 2013) aim at identifying a system characteristic

E. Di Lorenzo (✉) • S. Manzato
Siemens Industry Software (SISW), Interleuvenlaan 68, 3001 Leuven, Belgium
e-mail: emilio.dilorenzo@siemens.com; simone.manzato@siemens.com

W. Ostachowicz et al. (eds.), *MARE-WINT*, DOI 10.1007/978-3-319-39095-6_10

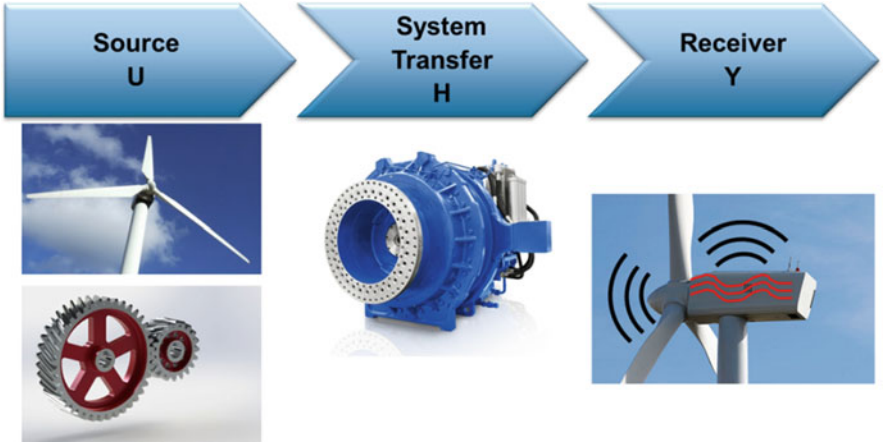

Fig. 10.1 The Source-Transfer-Receiver approach applied to a wind turbine gearbox

model based on input/output dynamic measurements. By identifying the origin of each of the phenomena of interest, it is possible to understand where corrective action should be applied increase the system NVH performances. Additionally, the identification of a system characteristic model will allow designer to compare experimental and numerical models using similar quantities. This approach will objectively quantify the agreement between the design assumptions and the behavior of the real structure.

The method is based on the so-called Source-Transfer-Receiver approach, as shown in Fig. 10.1 for a wind turbine gearbox. Experimental Modal Analysis relies on measurements of the system response at the receiver (i.e. acceleration) due to the measured inputs at the sources (typically forces) to identify a System Transfer function which represent the dynamics of the system itself. Modal Analysis will try to represent the information in the measured system transfer as natural frequencies, damping ratios and mode shapes. During operations, however, measuring the forces into the system can be practically impossible (for a gearbox, these are the loads transmitted from the whole turbine via the main shaft and the gearbox supports as well as the internal gear contact forces). Methods have been developed to overcome this limitation and thus allow to identify the modal properties of a system also in operating conditions, provided some assumption on the forces acting on the systems are verified (Peeters et al. 2007; Carne and James 2010). However, the main forces acting on a gearbox during operations appear at discrete frequencies multiple of the fundamental rotational speed. As one of the assumptions of Operational Modal Analysis is on the broadband spectrum of the forces, it is clear that identifying a modal model during stationary conditions is practically unfeasible for a gearbox, where the harmonic density is such that barely any mode is visible (Manzato et al. 2013).

However, during transient operations such as run ups and run downs, the rotational speed, and consequently its harmonics, is varying during the measurement. The different orders are then sweeping in a frequency band which is related to the minimum and maximum rotational speeds. As it happens during a sine sweep test, whenever one of these orders crosses a resonance, the response will increase accordingly. Orders can then be considered as representative of the system transfer (Fig. 10.1) and modal parameters identification techniques can be applied. The method was first introduced few years ago as Order based Modal Analysis (Janssens et al. 2006) and was further developed and validated recently. In this section, the concept of the method will be reviewed, with particular focus on the techniques required to extract orders that can be successfully used for modal analysis. Moreover, it will be positioned against standard Operational Modal Analysis techniques, showing the clear advantages in identifying reliable modal models of operating rotating machines and in particular for the wind turbine gearbox case.

As already discussed, the identification of operational modal model will allow not only to characterize the dynamic response of a structure in operating conditions, but will also provide means of validating, and subsequently updating, global numerical models developed with Multi Body and Finite Element tools, as demonstrated in Goris et al. (2013).

10.2 Order Tracking Techniques

Order tracking is the analysis of frequency components whose frequency is related to the rotational frequency of the operating machine. If the machine is running in non-stationary conditions, then the frequency components will be time varying and some more information are needed in order to perform the analysis. The additional information are in the form of tachometer signals measured on reference shafts of the machine. Several methods have been employed to digitally track orders which results from rotating components in noise and vibration problems (Blough 1998). In order to allow the computation of the exact frequency for the orders of interest, an accurate tachometer signal is needed for all the methods discussed in this section:

- Time domain sampling Fast Fourier Transform (FFT) order tracking;
- Angle domain computed order tracking;
- Time Variant Discrete Fourier Transform (TVDFT);
- Vold-Kalman (VK) filter based order tracking.

10.2.1 Time Domain Sampling-Based Fast Fourier Transform Order Tracking

The simplest digital order tracking techniques are based on the FFT on time domain data. These methods require time domain data sampled with a constant Δt (Fig. 10.2). The method performs a sliding FFT on time domain data and calculates the average rpm over which the transform is performed. This averaged rpm is then used for estimating the frequency of the orders of interest for each estimated spectra. Finally, the amplitude and the phase of the order are extracted from the FFT spectra. The order itself will not always fall on a single spectral line, so normally multiple spectral lines are summed. The FFT kernels are given in Eqs. (10.1) and (10.2), where $x(n\Delta t)$ is the nth discrete data sample, f_m is the frequency of the sine/cosine terms and a_m and b_m are the estimated Fourier coefficients:

$$a_m = \frac{1}{N}\sum_{n=1}^{N} x\,(n\Delta t)\cos\left(2\pi f_m n\Delta t\right) \tag{10.1}$$

$$b_m = \frac{1}{N}\sum_{n=1}^{N} x\,(n\Delta t)\sin\left(2\pi f_m n\Delta t\right) \tag{10.2}$$

The main advantage of this method is its computational efficiency. However, an important limitation is the constant time over which the transform is performed, regardless of the rpm of the machine. Additionally, it is assumed that all the sinusoidal functions are constant in amplitude over the time that the transform is performed. A leakage error is also present as orders are estimated by using an FFT based approach and a Hanning window is typically applied in order to reduce this effect.

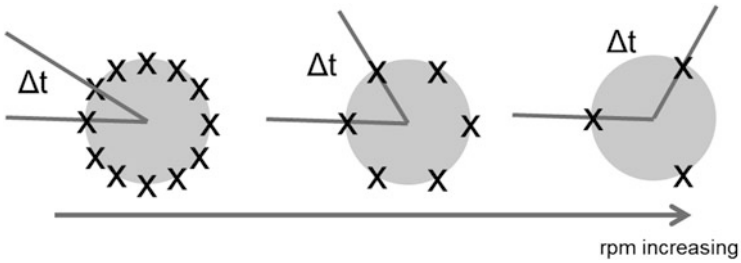

Fig. 10.2 Time domain sampling based FFT order tracking representation

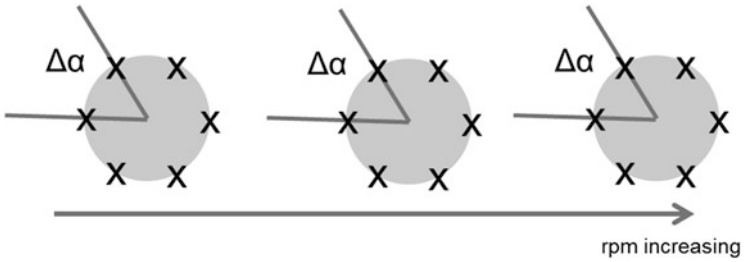

Fig. 10.3 Angle domain order tracking representation

10.2.2 Angle Domain Resampling Order Tracking

A very well-known order tracking method which is widely used in commercial software is based on angular resampling. Data are acquired with a uniform Δt and then resampled to the angle domain through the use of an adaptive digital resampling algorithm. The final result of the technique is that uniform Δt data become uniformly spaced angle data (Fig. 10.3). Estimates of amplitude and phase of the orders are obtained by processing these data with a Discrete Fourier Transform (DFT) instead of a FFT for computational flexibility in performing the transform without being restricted to a power of two number of samples.

In order to perform the transformation from time domain data to angle domain data, a reference signal has to be selected to define the instant of time in which the uniform angular intervals have been spaced. Typically, this signal is considered to be the tachometer signal measured on a reference shaft of the operating machine. The kernels of the Fourier transform are reformulated as shown in Eqs. (10.3) and (10.4), where o_m is the order which is being analyzed:

$$a_m = \frac{1}{N}\sum_{n=1}^{N} x\left(n\Delta\theta\right)\cos\left(2\pi o_m n\Delta\theta\right) \tag{10.3}$$

$$b_m = \frac{1}{N}\sum_{n=1}^{N} x\left(n\Delta\theta\right)\sin\left(2\pi o_m n\Delta\theta\right) \tag{10.4}$$

The advantages of the resampling based order tracking are leakage free estimates of orders which fall on spectral lines as well as an order resolution which is constant in terms of width. On the other hand, also this method has several restrictions. Orders may only be tracked with reference to one rotating shaft and it is very difficult to distinguish among order which cross one another. Another limitation is due to the finite defined order resolution which makes very difficult the analysis of orders which do not fall on a spectral line.

10.2.3 Time Varying Discrete Fourier Transform (TVDFT)

The Time Variant Discrete Fourier Transform (TVDFT) method gives results very similar to the resampling based order tracking, but with less computational efforts. It is based on a Fourier transform kernel whose frequency is varies with time and it does not require the transformation from the time to the angle domain (Blough et al. 1997). The TVDFT is based on kernels in which the sine and cosine functions have unity amplitude and an instantaneous frequency matching that of the tracked order at each instant in time, as shown in Eqs. (10.5) and (10.6):

$$a_m = \frac{1}{N}\sum_{n=1}^{N} x\left(n\Delta\theta\right)\cos\left(2\pi\int_0^{n\Delta t}\left(o_m * \Delta t * rpm/60\right)dt\right) \tag{10.5}$$

$$b_m = \frac{1}{N}\sum_{n=1}^{N} x\left(n\Delta\theta\right)\sin\left(2\pi\int_0^{n\Delta t}\left(o_m * \Delta t * rpm/60\right)dt\right) \tag{10.6}$$

The formulation can be extended in order to separate close or crossing orders through a secondary calculation. There can be a leakage error using the TVDFT with constant Δt sampled data because it is not guaranteed that the integer revolution values required for a constant order bandwidth analysis will fall on a Δt. If it is not the case, it will lead to a leakage error by performing the transformation over a non-integer number of revolutions. This error can be reduced by oversampling the data to finer Δt. The method retains most of the advantages of the resampling based order tracking and it can be implemented in a very efficient manner without having the computational load and complexity of the transformation from the time domain to the angle domain.

10.2.4 Vold-Kalman (VK) Filter-Based Order Tracking

Vold and Leuridan (1993) introduced an algorithm for high resolution, slew rate independent order tracking based on the concepts of Kalman filtering. The Vold-Kalman (VK) algorithm allows tracking multiple orders at the same time and it is able to decouple close and crossing orders. This method extracts the time history of the order as well as the estimate of the amplitude and the phase of the same order.

As the Kalman filter is based on the process and measurement equations, the VK filter is based on the structural and data equations. The structural equation describes the mathematical characteristics of the order to be extracted. It relies on information from the tachometer signal and represents a sine wave whose frequency and amplitude are constant over three consecutive points. To account for deviations

from a perfect sine wave over the considered time samples, a non-homogeneity term $\varepsilon(n)$ is introduced on the right-hand side of Eq. (10.7):

$$x(n) - 2\cos(\omega\Delta t)\, x(n-1) + x(n-2) = \varepsilon(n) \tag{10.7}$$

where $x(n)$ represents the nth discrete time sample and ω the instantaneous frequency of the sine wave. The second equation of the VK method is the so called data Eq. (10.8) and describes the relationship between the order $x(n)$ and the measured data $y(n)$. Normally the measured data are a combination of all orders generated in the machine plus a random noise component. This random noise, as well as the non-tracked orders, are then combined into the signal $\eta(n)$:

$$y(n) = x(n) + \eta(n) \tag{10.8}$$

A weighted solution is obtained by introducing the Harmonic Confidence Factor (HCF) r. This value determines the tracking characteristic of the filter and is calculated according to Eq. (10.9) as the ration between the standard deviations of the structure and data equations:

$$r(n) = \frac{s_\varepsilon(n)}{s_\eta(n)} \tag{10.9}$$

Choosing large values of r leads to a highly selective filtering in the frequency domain; on the contrary, small values will decrease the frequency resolution while obtaining faster convergence. By applying the ratio as a weighting function and combining the two previous equations, the system in Eq. (10.10) is obtained:

$$\begin{bmatrix} 1 & -2\cos(\omega\Delta t) & 1 \\ 0 & 0 & r(n) \end{bmatrix} \begin{bmatrix} x(n-2) \\ x(n-1) \\ x(n) \end{bmatrix} = \begin{bmatrix} \varepsilon(n) \\ r(n)y(n) - \eta(n) \end{bmatrix} \tag{10.10}$$

Applying Eq. (10.10) to all observed time samples will give a global system of over-determined equations for the desired waveform $x(n)$ that can be easily solved with standard least square techniques. For the specific case of order tracking, the filtered waveform is most conveniently described in terms of amplitude and phase with respect to a reference channel such as the tachometer.

10.3 Order-Based Modal Analysis

Operational Modal Analysis (OMA) algorithms, such as Operational Polymax (Peeters et al. 2007), allow the identification of the modal parameters of a structure by taking into account only operational measurements. However, when applied to data acquired during transient phenomena, such as run ups and coast down, data

need to be carefully interpreted. Input data for the modal parameter identification process are auto and cross spectra calculated from the complete time histories and assuming the excitation can be considered broad-band white noise. However, when spectra are calculated on run up data of rotating machineries, sharp peaks appears at fixed intervals. These peaks relate to the so-called "end-of-order" effect and originate from order components suddenly stopping at the maximum rpm. When using this spectra in standard OMA, they will be erroneously identified as physical poles from the algorithm; additional, they can hamper the accuracy in the estimation of modes at nearby frequencies.

The idea of performing OMA on tracked orders instead of considering the spectra arose because, during a run-up or run-down test, the measured response are mainly caused by the rotational excitation. In this formulation, the run-up or run-down is then considered as a multi-sine sweep excitation in the frequency band of interest. The excitation force acting on the structure is considered to be equivalent to that of a rotating mass with increasing (or decreasing) frequency, which can be represented as two correlated perpendicular forces of equal amplitude and in quadrature (90° phase difference). The measured structural response can then be represented in the frequency domain as shown in Eq. (10.11) where the terms F relate to the forces while the H indicate the corresponding columns in the transfer function matrix:

$$Y(\omega) = H_{(:,f_x)}(\omega) F_x(\omega) + H_{(:,f_y)}(\omega) F_y(\omega) \tag{10.11}$$

Taking into account the relation between the two perpendicular rotating forces and considering only the positive frequency axis, Eq. (10.12) is obtained:

$$Y(\omega) \propto \omega_0^2 \left(H_{(:,f_x)}(\omega) - jH_{(:,f_y)}(\omega) \right) \delta(\omega - \omega_0) \tag{10.12}$$

where ω_0 is the rotation speed. This equation shows that the measured output is proportional to the squared rotation speed and to a complex combination of two structural FRFs related to x and y excitation. In general, a structural FRF can be modally decomposed as shown in Eq. (10.13):

$$H_{(:,\bullet)}(\omega) = V(j\omega I - \Lambda)^{-1} L_\bullet + \frac{1}{\omega^2} LR_\bullet + UR_\bullet \tag{10.13}$$

where LR and UR are the real-valued lower and upper residuals which are used for modeling the influences of the modes outside of the considered frequency band. V, Λ and L are the mode shape matrix, the diagonal matrix containing the complex poles and the modal participation factors. Equations (10.11) and (10.13) show that modal analysis can be applied to displacement orders taking into account that:

- Displacement orders are proportional to the squared rotation speed and, as a consequence, acceleration orders are proportional to the forth power of the same rotation speed. The main difference is that in the classical modal analysis the acceleration FRFs are proportional to the squared frequency axis.

- Upper and lower residuals are complex, while in classical modal analysis they are real.
- Participation factors are complex both in classical and order based modal analysis.

Methods such as Operational Polymax and Operational Polymax Plus are robust again these observations and they can be employed for estimating the modal parameters in case of rotating machineries by looking at the orders rather than at the spectra.

10.4 Dynamic Characterization of Operational Gearboxes

With the main objectives of characterizing the gearbox dynamic response in different operating conditions and obtaining experimental data for model validation and updating, a measurement campaign took place on the 13.2 MW dynamic test rig at ZF Wind Power in Lommel, Belgium (Fig. 10.4). Using this test rig, gearboxes can be tested under representative loading condition using parameterized load cases that can be programmed into the test rig controller. In this case, the following scenarios were tested:

- Shaker sine sweep during standstill and in stationary operating conditions at 1200 rpms.
- Stationary operating conditions at 1200 and 800 rpms.
- Run up from 200 to 1500 rpms with a speed of 5 rpms/s.
- The operational measurements were all repeated under different torque loading (33 %, 66 % and 100 % of nominal torque).

As shown in Fig. 10.4 (right) an extensive grid of 250 points on both the gearboxes and the test rig was measured using tri-axial accelerometers. To measure all points, the whole test schedule was repeated 7 times roving the available sensors to cover the whole grid. To ensure the data form the different dataset could be

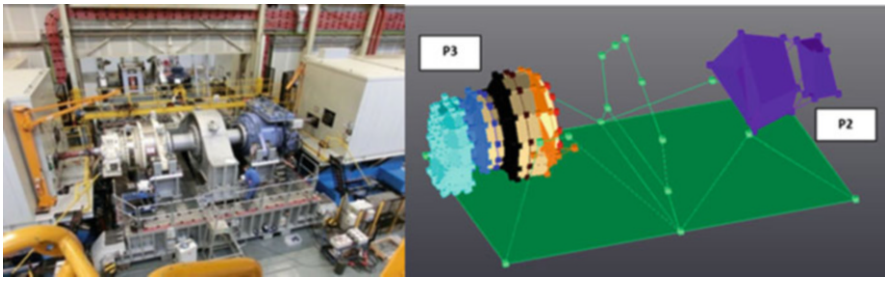

Fig. 10.4 Test-rig configuration (*left*); markers identifying the measurement points on the test-rig (*right*)

compared, a set of 7 single axis accelerometers was always kept in the same positions. 3 optical sensors (zebra tape + laser) were respectively installed on the Low Speed Shaft and at the High Speed Shaft of each of the two gearboxes in the test rig.

With the objective of comparing the modal parameters obtained in different operating conditions, data measured during shaker excitation with the gearbox in standstill conditions have been analysed. After computing Frequency Response Functions, standard Experimental Modal Analysis methods were applied and a set of reference modal parameters obtained (Manzato et al. 2015). A similar processing was also performed on the data collected applying the sine sweep via the shaker during stationary operations. However, although some of the modes could still be identified, it was concluded that the shaker were not powerful enough to sufficiently excite the structure and ensure a reliable modal estimation.

Response data acquired during acceleration measurement were also acquired and the signature of the gearbox during operation at constant speed is shown in Fig. 10.5.

All vertical lines in the time-frequency diagram represent highly excited harmonics of the fundamental rotational speed and they can all be related to rotational speed of the shafts of the different stages as well as to the gear meshing frequencies. As the response is dominated by narrow and closely spaced harmonic components, standard Operational Modal Analysis cannot be applied. As a consequence, to understand the response, only Operational Deflection Shapes can be analysed, but, as mentioned, it will be impossible to understand whether the high response at the receiver is due to the system or the source (Fig. 10.1). Of course one could compare the harmonic frequency with the natural frequencies identified by applying shaker excitation in stationary conditions. However, as the boundary conditions

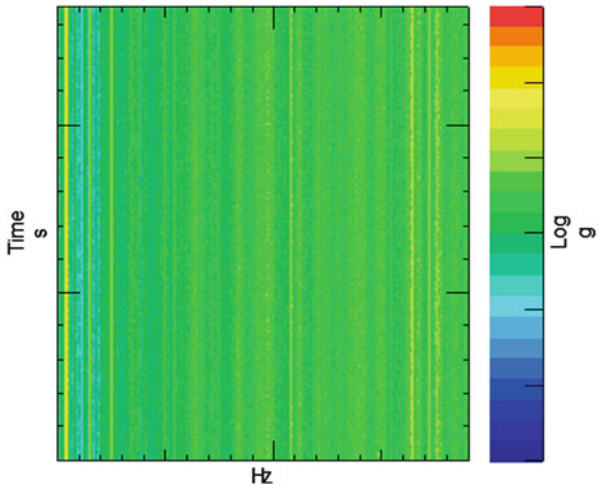

Fig. 10.5 Signature of the gearbox on the test rig during stationary operations

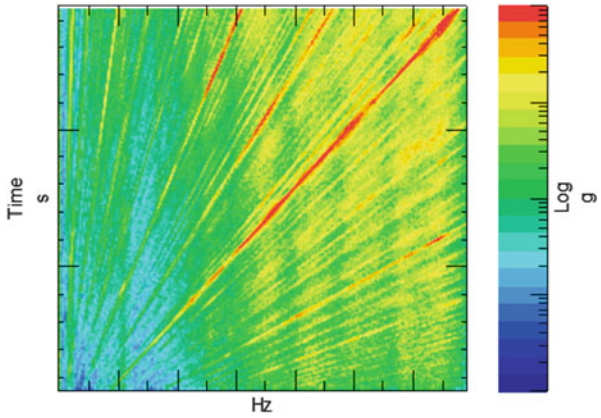

Fig. 10.6 Signature of the gearbox on the test rig during a run-up at 5 rpm/s

between standstill and operational conditions are significantly different, erroneous conclusion might be derived.

The signature obtained during a run up is significantly different and is shown in Fig. 10.6. In this case, the different orders vary in frequency and the resulting excitation is similar to that of a multi-sine sweep. As will be explained in the next sections, both Operational and Order-based Modal Analysis can be applied to these data to extract the modal parameters.

10.4.1 Operational Modal Analysis

Operational Modal Analysis requires as input data acceleration auto and cross-spectra calculated using the complete time history. The results can then be considered as an average over time of the frequency response shown in Fig. 10.5. By combining the response at the different orders, the resulting spectra can be considered as the response to a "flat" broadband excitation, thus complying with the OMA assumption. The resulting spectra are shown in Fig. 10.7. Although the spectrum shown is suitable for OMA processing, the results might be wrongly interpreted if the data are not carefully analysed.

A comparison of the two graphs reveals that some of the peaks in the spectrum (and in particular the sharpest ones) originate from order components suddenly stopping at the maximum rpms. Cursors were added to the pictures at frequencies that were identified as poles of the gearbox by classical OMA. Moreover, as the two gearboxes on the test rig were slightly different prototypes, they rotate at slightly different speeds, resulting on a doubling of these "end-of-order" related poles. This is the main weakness of this method: not only the real poles are identified, but also the so-called "end-of-order" related poles which are physically not present

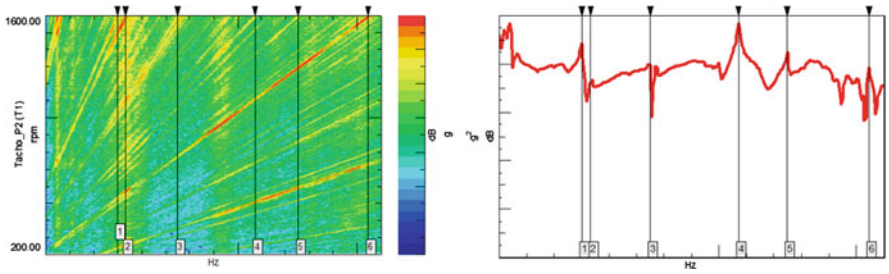

Fig. 10.7 RPM-frequency spectrogram of the gearbox run up and corresponding spectrum

in the system and are purely processing artifact. The four identified frequencies correspond to some of the main order components ending at that frequency. The estimated modal model is consequently not correct because it considers them as poles of the system. While these poles could be ignored a-posteriori, in cases were many orders are present (such as this one) they can also affect the estimation of close modes, thus reducing the confidence in the identified model.

10.4.2 Order-Based Modal Analysis

The conclusions from Sect. 10.4.1 motivated the development of a new method able to reliably identify a modal model of a rotating machine during operation. Instead of applying modal parameter identification on the spectra, the concept is to identify the dominant orders in the response and then use them to extract the modal parameters in the frequency band the span. The process to perform Order-based Modal Analysis is displayed in Fig. 10.8. The first two steps pre-process the tacho data to remove spikes that could be present in the signal and make it smoother. Once the tacho is corrected, order tracking can be applied using one of the techniques discussed in Sect. 10.2 and the orders of interest extracted. On each of these orders operational modal identification can then be applied and the modal parameters from the different orders combined to obtain the modal response in the frequency band of interest.

As an example, Fig. 10.9 compares the cross-power spectrum and the 1st order of the high speed gear stage order (1st gear mesh frequency of the High Speed Stage) for the same channel over the same frequency bandwidth. The order is estimated using two of the techniques presented in Sect. 10.2, namely the Time varying Discrete Fourier Transform (TVDFT) and the Vold-Kalman filter (VK). It can be observed that, while the cross spectrum on the left spans the complete frequency band, the order only start from a higher minimum frequency. To span the full bandwidth, different orders need to be extracted and the modes identified.

Applying the classical OMA processing (see Sect. 10.4.1) and using the Operational Polymax algorithm, 13 modes are identified in the frequency band between 80 and 400 Hz. The same processing was repeated for different load levels to

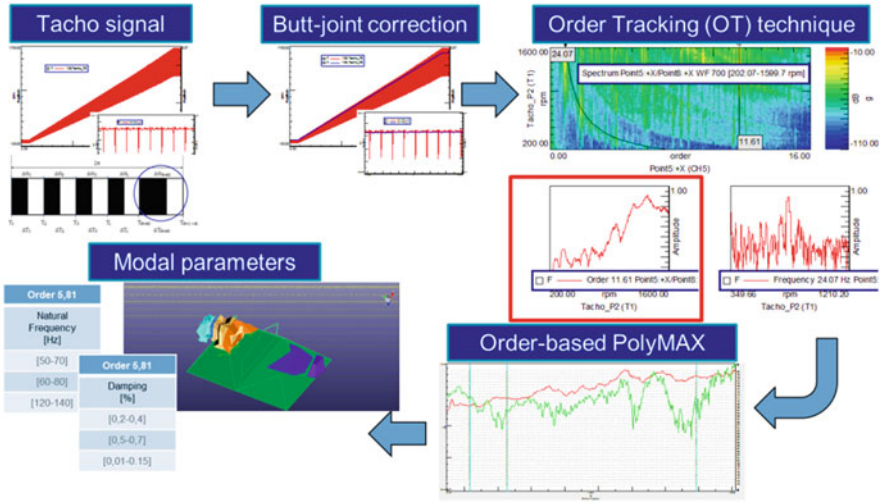

Fig. 10.8 Order-based Modal Analysis process overview

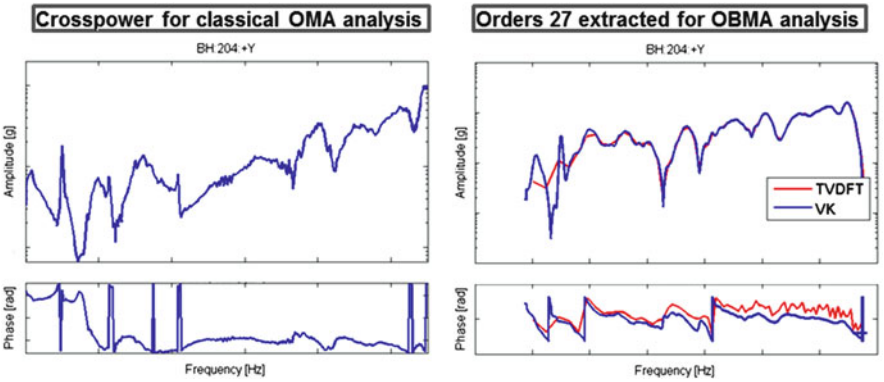

Fig. 10.9 Crosspower for classical OMA analysis (*left*) and 1st high speed gear stage order extracted by using two different order tracking techniques for OBMA analysis (*right*)

investigate possible system non-linearities resulting in variations of modal parameters. The results are summarized in Fig. 10.10, where the relative variations of the natural frequencies for the 3 cases (using as reference load case the one with 100 % load) are displayed. The general trend from the results shows an increase of the natural frequencies with the torque value. Generally, almost all modes are consistently identified in the 3 load cases, but it should be noted that the majority of them actually represent "end-of-order" poles.

By first extracting the orders with the TVDFT and VK tracking algorithms from the same time data and then using these orders for OBMA, the results shown in Figs. 10.11 and 10.12 are obtained.

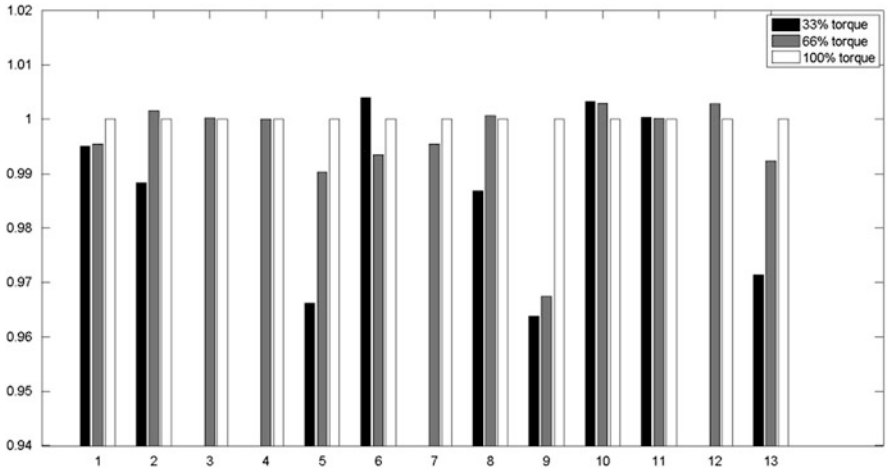

Fig. 10.10 Operational Modal Analysis results on run up data—relative variation of natural frequencies with torque level

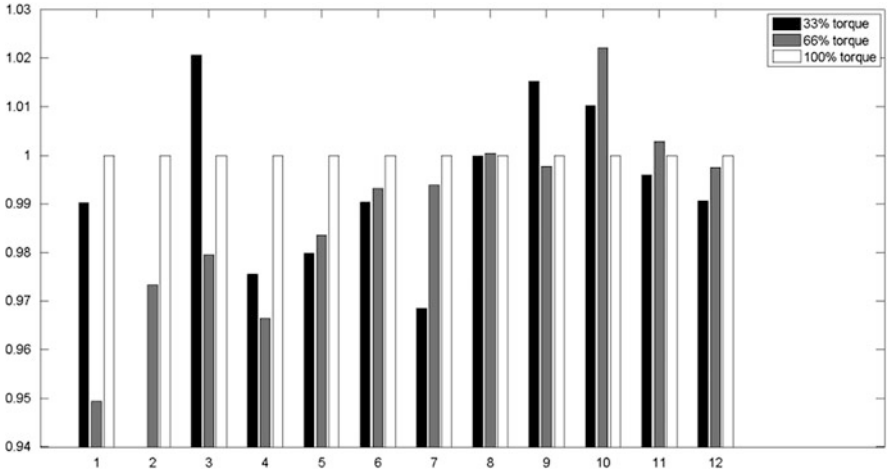

Fig. 10.11 Order-based Modal Analysis with TVDFT order tracking—relative variation of natural frequencies with torque level

From the displayed results it is immediately clear that OBMA on the VK tracked orders is the process which identifies the highest number of modes. One way of validating the identification results is to compare the measured order with the one computed using the modal parameters in the parameterization of the system transfer presented in Eq. (10.13). The synthesized models from OBMA using the two selected order tracking techniques are shown in Fig. 10.13. In the mid-high frequency band, the identified modal models are able to accurately replicate the measured order. However, at lower frequencies, where the number

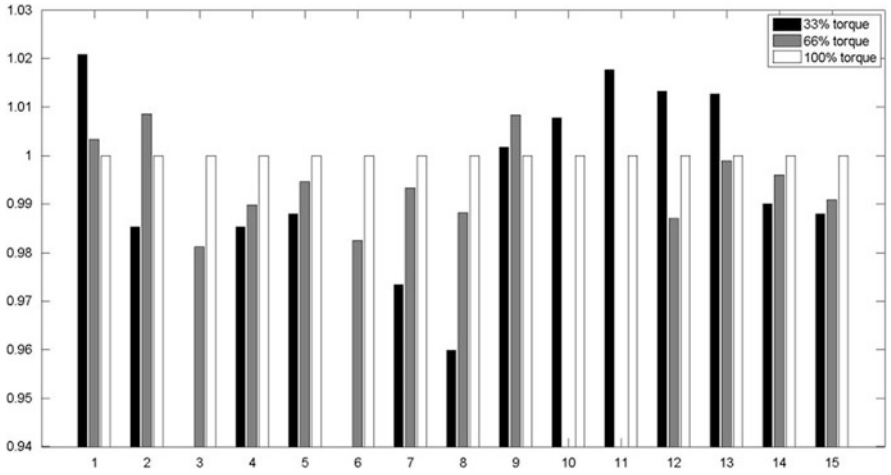

Fig. 10.12 Order-based Modal Analysis with VK order tracking—relative variation of natural frequencies with torque level

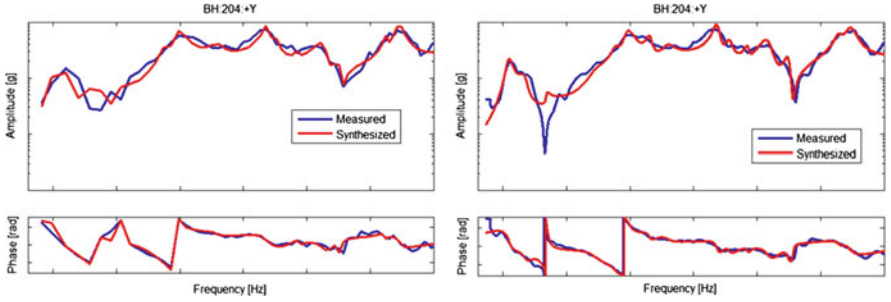

Fig. 10.13 Measured vs. synthesized orders by using OBMA with TVDFT (*left*) and VK (*right*) order tracking

of available samples for the order estimation is typically smaller, VK as expected performs significantly better. By applying OMA on the data, the results displayed in Fig. 10.14 are obtained. The difference between the measured and synthesized curve is now immediately evident and the identified model is thus not able to represent the true measured response. Also, the majority of the identified peaks appear very sharp and they correspond to end-of-order poles.

Finally, a further comparison between the different methods can be performed by computing the Modal Assurance Criterion (MAC) between mode sets. The results for different combinations of mode sets are displayed in Fig. 10.15: values of MAC equal to 1 (Red) mean two modes are perfectly correlated, while a MAC of 0 (Blue) means the two vector are perfectly orthogonal.

The displayed results focus on the results obtained for the 100 % load cases using the three different discussed methods. Only few modes are found to be similar

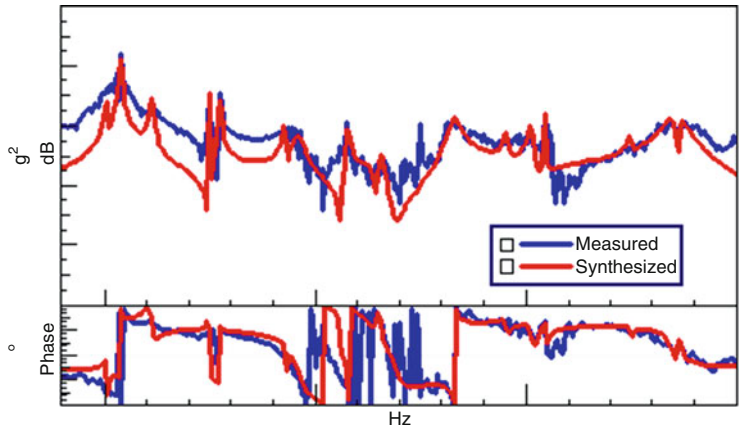

Fig. 10.14 Measured vs. synthesized crosspower spectra using classical OMA

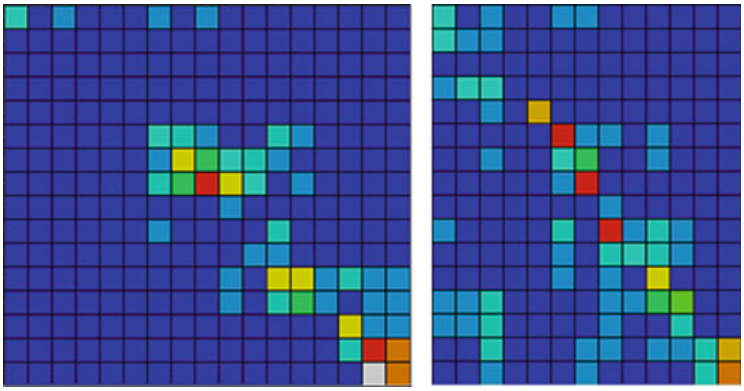

Fig. 10.15 MAC comparisons. *Left*: OMA vs. OBMA-VK; *right*: OBMA-TVDFT vs. OBMA-VK

between OMA and OBMA and this is related to the high number of end-of-order poles identified. By comparing the results obtained using the two order tracking techniques, a discrete correlation is found for the modes in the mid-high frequency range. As expected from the results displayed also in Fig. 10.12, at lower frequencies the predicted orders differ significantly, thus a difference in the extracted modes is also expected.

Table 10.1 summarizes the differences between the analyzing order tracking techniques by analyzing:

- the input parameters the user has to define.
- the computational effort required for the estimation.

Table 10.1 Critical assessment of the different analyzed order tracking techniques

Order tracking technique	Advantages & drawbacks
Angle Domain Order Tracking	Suitable for real-time processing Equidistant order lines Huge number of parameters to be set Great sensitivity of the resulting order on the settings Very noisy phase Modal parameter estimation is not reliable
Time Variant Discrete Fourier Transform	1 parameter to be set (number of rotation per order line) Computationally efficient Post-calculation to separate close and crossing orders Non equidistant order lines Low resolution at low frequency Phase smoothness depends strongly on the number of rotation per order line Difficult to fit higher frequency
Vold-Kalman Filter Order Tracking	2 parameters to be set (filter bandwidth and number of poles in the filter) Very high order resolution (number of lines equal to the number of acquired samples) Very good quality of the fit Beat free extraction of close and crossing orders Tracking capabilities are independent of the slew rate Non equidistant order lines Computationally demanding

The performed comparison also includes standard Angle-domain resampling order tracking. Although the results are not discussed here, the method is one of those most employed in industry and implemented in commercial solutions.

Figures 10.16 and 10.17 show the comparison between the same mode obtained by applying the OMA and OBMA techniques. In Manzato et al. (2015), the same results were also compared with the modes identified with shaker excitation. In terms of natural frequencies, the different techniques correlate very well.

On the other hand, damping values are more scattered, which is however expected with operational data. However, when comparing mode shapes using the Modal Assurance criterion, very poor correlation is observed although the shapes graphically compare. These results can be however be expected by taking into account the number of measurement points, the measurement and processing noise and uncertainties as well as the small inconsistencies between the different runs where the setup was changed.

Thus, at least when these conditions apply, it is envisaged to validate the analysis only qualitatively by comparing the mode shapes rather than performing a quantitative analysis based on the MAC.

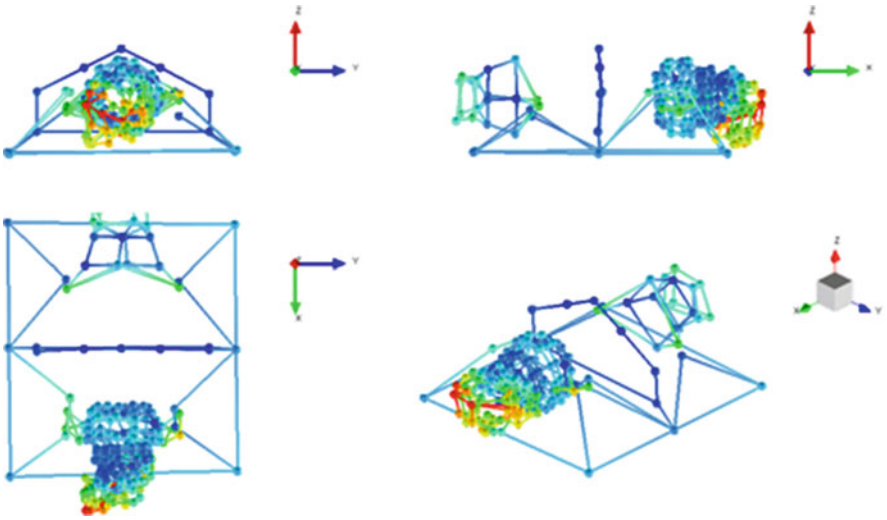

Fig. 10.16 OMA results—Deformed shape of mode #9

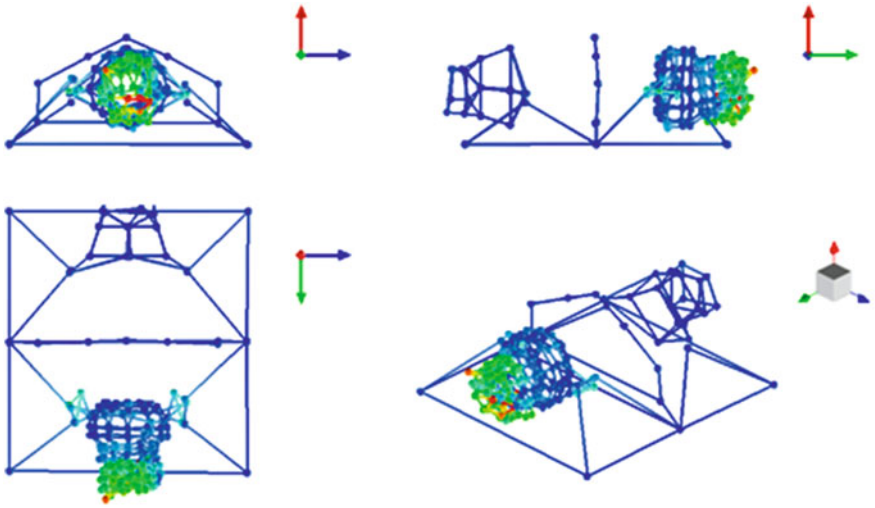

Fig. 10.17 OBMA-VK results—Deformed shape of mode #9

10.5 Conclusions

When analysing the dynamic response of rotating machines in operating conditions, the techniques developed to perform operational modal analysis don't hold. After clearly demonstrating that these methods don't provide reliable results both during

stationary and transient condition, a novel method is introduced, which is able to extract an operational modal model from run-up or run-down experiments.

Order-Based Modal Analysis (OBMA) relies on extracting high quality order from the throughput time data that can be then used for modal parameter identification using classical operational modal analysis algorithm. The advantages over classical Operational Deflection Shape (ODS) that also rely on order extraction are the possibility to clearly identify which part of the response can be associate to the system dynamics, which to the input forces and which to a combination of both. Moreover, damping information for each of the modes can be extracted and closely separated modes, as soon as the order resolution allows it, can be distinguished.

However, the use of an accurate phase reference signal is mandatory to obtain a reliable modal model and because of this an accurate tacho measurement is even more critical than in standard ODS analysis. Also, by using more advanced order tracking techniques, although sometimes computationally demanding, can lead to significant improvement of the results.

OBMA has demonstrated to be suitable for operational processing and to give very good results. The method was significantly improved and the two new methods (TVDFT and VK) showed much improved results compared to older implementations. The extra effort compared to calculate the ODS are limited, although the Vold-Kalman order tracking is computationally more demanding and the quality of the tacho signal should be high enough to allow a reliable processing of the data. The results of the proposed approach were used in Vanhollebeke et al. (2015) to validate the operational response of the analysed gearbox predicted using a flexible multibody model.

Acknowledgments The authors would link to kindly acknowledge Frederik Vanhollebeke, Sonja Goris and Joris Peeters of ZF Wind Power for the possibility of using the data acquired on the gearbox test rig to carry out this research. Additionally, the authors kindly acknowledge the Institute for Promotion of Innovation through Science and Technology in Flanders, Belgium (IWT Vlandereen) for the O&O grant ALARM in which the aforementioned experimental campaign was performed. The ALARM project was furthermore supported by an Eureka label in the framework of international co-operations.

References

Blough J (1998) Improving the analysis of operating data on rotating automotive components. Dissertation, University of Cincinnati

Blough J, Brown DL, Vold H (1997) The time variant discrete fourier transform as an order tracking method. In: Publications: Technical Paper Number 972006. Society of Automotive Engineers. Available via SAE. http://papers.sae.org/972006/. Accessed 08 Apr 2016

Carne TG, James GH III (2010) The inception of OMA in the development of modal testing for wind turbines. Mech Syst Signal Pr 24:1213–1226

Goris S, Vanhollebeke F, Ribbentrop A et al (2013) A validated virtual prototyping approach for avoiding wind turbine tonalities. Paper presented at the 5th international conference on wind turbine noise, INCE-Europe, Denver, 28–30 August 2013

Heylen W, Lammens S, Sas P (2013) Modal analysis theory and testing. KU Leuven, Belgium

Janssens K, Kollar Z, Peeters B et al (2006) Order-based resonance identification using operational Polymax. In: Abstracts of the IMAC-XXIV: conference and exposition on structural dynamics – looking forwards: technologies for IMAC, Society for Experimental Mechanics, St. Louis, 30 January–02 February 2006

Manzato S, White JR, LeBlanc B et al (2013) Advanced identification techniques for operational wind turbine data. In: Allemang R, De Clerck J, Niezrecki C et al (eds) Topics in modal analysis volume 7: proceedings of the 31st IMAC, a conference on structural dynamics, 2013. Conference Proceedings of the Society for Experimental Mechanics Series, Springer, New York

Manzato S, Di Lorenzo E, Medici A et al (2015) Order-based modal analysis versus standard techniques to extract modal parameters of operational wind turbine gearboxes. In: Mains M (ed) Topics in modal analysis volume 10: proceedings of the 33rd IMAC, a conference and exposition on structural dynamics, 2015. Conference Proceedings of the Society for Experimental Mechanics Series, Springer, New York

Peeters B, Van der Auweraer H, Vanhollebeke F et al (2007) Operational modal analysis for estimating the dynamic properties of a stadium structure during a football game. Shock Vib 11:395–409

Vanhollebeke F, Peeters P, Helsen J et al (2015) Large scale validation of a flexible multibody wind turbine gearbox model. J Comput Nonlinear Dynam. doi:10.1115/1.4028600

Vold H, Leuridan J (1993) High resolution order tracking at extreme slew rates, using Kalman tracking filters. In: Publications: Technical Paper Number 931288. Society of Automotive Engineers. Available via SAE. http://papers.sae.org/931288/. Accessed 08 Apr 2016

Part III
Tower & Support Structure